Biogenesis of cytochromes *c* and c_1 in the electron transport chain of malaria parasites

Aldo E. García-Guerrero, Rebecca G. Marvin, Amanda Mixon Blackwell, and Paul A. Sigala*

Department of Biochemistry, University of Utah School of Medicine, Salt Lake City, UT, USA

*Corresponding author: Paul Sigala

E-mail: p.sigala@biochem.utah.edu

Keywords: *Plasmodium falciparum*, malaria parasites, electron transport chain, mitochondria, cytochrome c, heme metabolism, holocytochrome c synthase, drug target

ABSTRACT

Plasmodium malaria parasites retain an essential mitochondrional electron transport chain (ETC) that is critical for growth within humans and mosquitoes and a key antimalarial drug target. ETC function requires cytochromes *c* and c_1 that are unusual among heme proteins due to their covalent binding to heme via conserved CXXCH sequence motifs. Heme attachment to these proteins in most eukaryotes requires the mitochondrial enzyme holocytochrome *c* synthase (HCCS) that binds heme and the apo cytochrome to facilitate biogenesis of the mature cytochrome *c* or c_1. Although humans encode a single bifunctional HCCS that attaches heme to both proteins, *Plasmodium* parasites are like yeast and encode two separate HCCS homologs thought to be specific for heme attachment to cyt *c* (HCCS) or cyt c_1 (HCC_1S). To test the function and specificity of *P. falciparum* HCCS and HCC_1S, we used CRISPR/Cas9 to tag both genes for conditional expression. HCC_1S knockdown selectively impaired cyt c_1 biogenesis and caused lethal ETC dysfunction that was not reversed by over-expression of HCCS. Knockdown of HCCS caused a more modest growth defect but strongly sensitized parasites to mitochondrial depolarization by proguanil, revealing key defects in ETC function. These results and prior heterologous studies in *E. coli* of cyt *c* hemylation by *P. falciparum* HCCS and HCC_1S strongly suggest that both homologs are essential for mitochondrial ETC function and have distinct specificities for biogenesis of cyt *c* and c_1, respectively, in parasites. This study lays a foundation to develop novel strategies to selectively block ETC function in malaria parasites.

Malaria remains a devastating infectious disease, especially in sub-Saharan Africa (1). The lack of a long-lasting, broadly protective vaccine and increasing resistance to frontline antimalarial drugs underscore the urgency to unravel the basic biology of malaria parasites to identify new vulnerabilities suitable for therapeutic targeting. Severe malaria is caused by *Plasmodium falciparum* parasites, which infect and grow asexually within human red blood cells (RBCs) to cause all malaria symptoms. RBCs contain an enormous amount of heme, and cellular metabolism involving this key cofactor is central to the biology of malaria parasites (2-4). During their 48-hour residence inside an RBC, parasites internalize and digest nearly 80% of the host-cell hemoglobin (5). This massive proteolysis releases abundant free heme, which parasites detoxify by formation of hemozoin crystals inside their digestive vacuole. This critical pathway is a major antimalarial drug target and is central to the activity of chloroquine and artemisinin, two of the historically most successful antimalarial drugs (6).

P. falciparum parasites also require heme as a metabolic cofactor to support key aspects of their cellular physiology, especially the mitochondrial electron transport chain (ETC) that is essential for all stages of parasite development in humans and mosquitoes (3, 4, 7). ETC activity is directly inhibited by the current antimalarial drug, atovaquone (8, 9), and the key vulnerability of this pathway in all parasite stages has made it the subject of intense drug discovery efforts (10-12). Multiple heme-dependent cytochromes (cyt) are critical for ETC activity and parasite viability, including cyt *b* and c_1 in Complex III, soluble cyt *c* that shuttles electrons between Complexes III and IV, and the heme A-binding Cox1 subunit of Complex IV (3, 13). In blood-stage parasites, the critical function of Complexes III and IV is oxidative recycling of the ubiquinone cofactor used as an electron acceptor by multiple mitochondrial dehydrogenases, especially dihydroorotate dehydrogenase required for pyrimidine biosynthesis (**Fig. 1**) (9, 14-16).

Although electron transfer through these two complexes is accompanied by proton translocation across the inner membrane, this proton-pumping activity is not directly essential for blood-stage parasites. *P. falciparum* has a redundant mechanism to polarize the mitochondrial inner membrane that is inhibited by proguanil, and blood-stage parasites rely on cytoplasmic glycolysis for ATP production rather than mitochondrial ATP synthase (9, 17). Of the known mitochondrial cytochromes, cyt *b* and Cox1 are encoded on the mitochondrial genome, which is not currently accessible to genetic modification. Cyt *c* (Pf3D7_1404100) and c_1 (Pf3D7_1462700), however, are encoded in the nucleus, and we recently demonstrated that both cytochromes are critical for blood-stage parasites and ETC function (16). *P. falciparum* and other apicomplexan parasites also encode a divergent cyt *c* paralog (cyt *c*-2, Pf3D7_1311700) that binds heme but whose function is dispensable for blood-stage parasites (16).

Mitochondrial cyt *c* and c_1, which are retained by nearly all aerobic eukaryotes, are distinguished from most heme proteins by their use of a conserved CXXCH sequence motif to covalently bind heme via formation of stable thioether bonds between the Cys residues and the heme vinyl groups (18-21). In most eukaryotes, the assembly of these heme-bound cytochromes requires the enzyme holocytochrome *c* synthase (HCCS) that is located on the outer leaflet of the inner mitochondrial membrane and whose activity has been best studied in yeast and humans (22, 23). Although hemylation of cyt *c* and c_1 is central to eukaryotic respiration, no structure has been determined experimentally for any mitochondrial HCCS from any organism. Nevertheless, recombinant expression and functional reconstitution of cyt *c* hemylation by human HCCS have enabled a proposed mechanism for heme attachment (23, 24). According to this mechanism, HCCS binds heme via a conserved His residue, binds the N-terminal α-helix of apo cyt *c*, and positions the bound heme proximal to the CXXCH residues to facilitate stereospecific heme attachment and

thioether bond formation to cyt *c.* These steps are followed by folding and release of mature cyt *c*. Although humans and other metazoans retain a single bifunctional HCCS that can hemylate both cyt *c* and c_1 (25), other eukaryotes express two distinct HCCS homologs that preferentially hemylate cyt *c* (HCCS) or cyt c_1 (HCC_1S) (22, 26). Nevertheless, studies in *Saccharomyces cerevisiae* (25) and the apicomplexan parasite *Toxoplasma gondii* (27) have suggested that HCCS in these organisms has limited promiscuous activity in hemylating cyt c_1, in addition to its preferred cyt *c* substrate.

P. falciparum also expresses both HCCS (Pf3D7_1224600) and HCC_1S (Pf3D7_1203600) homologs, but their functional properties have been sparsely studied. Genome-wide and targeted knock-out studies in *P. falciparum* and *P. berghei* have reported that both genes are refractory to disruption (28-30), suggesting non-redundant essential functions. Our prior work also indicated that parasite HCCS but not HCC_1S could hemylate cyt *c* or *c*-2 when expressed heterologously in *E. coli*, suggesting that each homolog is specific for hemylating cyt *c* or c_1, respectively (16). To directly test the function and specificity of HCCS and HCC_1S in *P. falciparum* parasites, we used CRISPR/Cas9 to tag each gene for conditional knockdown studies. Loss of HCC_1S impaired cyt c_1 biogenesis and resulted in lethal ETC dysfunctions that were not rescued by HCCS over-expression. Knockdown of HCCS led to a more modest phenotype but strongly sensitized parasites to mitochondrial depolarization by proguanil, unmasking a key ETC defect. These studies unravel non-overlapping essential functions for HCCS and HCC_1S in biogenesis of cyt *c* and c_1 in malaria parasites. Specificity differences between human and parasite HCCS homologs can provide a basis to develop selective inhibitors of ETC function in *Plasmodium*.

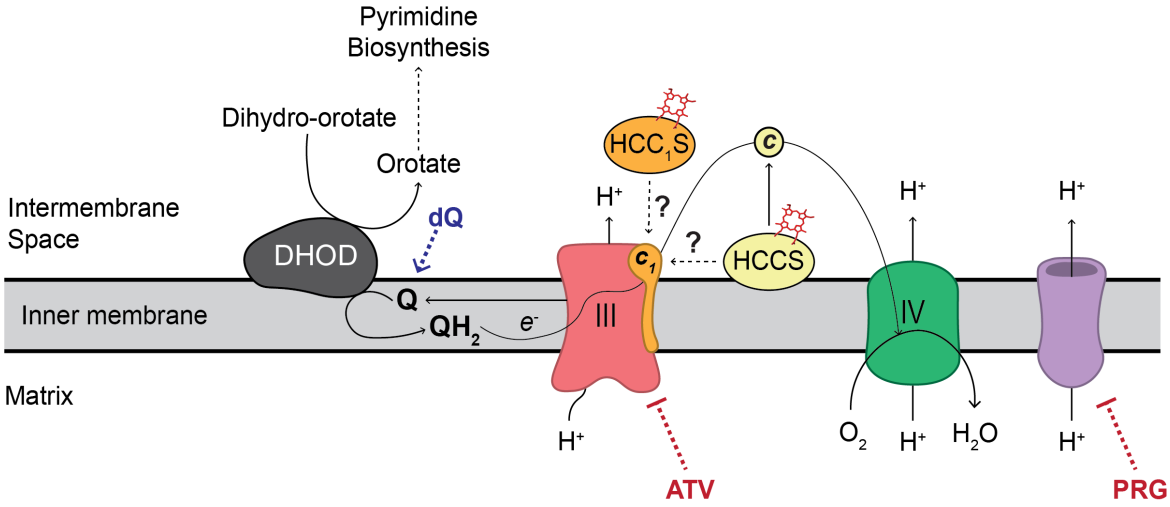

Figure 1. Schematic model of mitochondrial heme metabolism in *P. falciparum* parasites, focusing on the role of heme-dependent cytochromes *c* and c_1 in the electron transport chain. ATV = atovaquone, DHOD = dihydroorotate dehydrogenase, dQ = decyl-ubiquinone, Q = oxidized ubiquinone, QH_2 = reduced ubiquinol, III = Complex III/bc_1, IV = Complex IV/Cyt *c* oxidase, c = cyt *c*, c_1 = cyt c_1, HCCS = holocytochrome *c* synthase, HCC_1S, holocytochrome c_1 synthase, PRG = proguanil. Purple = alternative, proguanil-sensitive pathway for maintaining transmembrane potential. Question marks indicate functional uncertainty.

RESULTS

***P. falciparum* encodes HCCS and HCC_1S proteins homologous to yeast and humans.** To better understand the sequence features of the *Plasmodium* HCCS and HCC_1S homologs, we aligned these two proteins with HCCS orthologs from humans, yeast, and *Toxoplasma gondii* (**Fig. 2A**) and observed sequence identities ranging from 30-45%. *P. falciparum* HCCS (Pf3D7_1224600) had similar 35% and 38% sequence identity to yeast HCCS and HCC_1S, respectively. The parasite HCC_1S (Pf3D7_1203600), however, had higher sequence identity with yeast HCC_1S (41%) than yeast HCCS (30%), consistent with its predicted specificity for cyt c_1 and lack of detectable hemylation of cyt *c* in prior heterologous studies in *E. coli* (16). We also generated a maximum likelihood phylogenetic tree, based on alignment of the *Plasmodium* HCCS and HCC_1S proteins with 52 orthologs from diverse eukaryotes, that further supported functional divergence between the parasite homologs (**Fig. S1**).

Based on the alignment in Fig. 2A and in agreement with prior studies (23, 31), we observed multiple areas of strong sequence conservation between all orthologs that included the conserved His residues at H154 and H211 (Human HCCS numbering) and neighboring residues E159 and W162. H154 has previously been demonstrated in human HCCS to serve as a key axial ligand required for heme binding by HCCS and hemylation of cyt *c*, but a functional role for H211 remains undefined (23). E159 and W162 also contribute to heme binding, and E159 mutations underpin the human disease called micropthalmia with linear skin defects syndrome (31, 32). The high conservation in these and nearby residues between human and *P. falciparum* HCCS is consistent with our prior observation that each HCCS ortholog could promiscuously catalyze heme attachment to cyt *c* from both organisms (16).

No three-dimensional structure has been determined experimentally for a eukaryotic HCCS enzyme. As an initial step towards understanding structural features of HCCS, the positioning of conserved residues, and the possible orientation of HCCS bound to cyt *c* and its CXXCH heme-binding motif, we first turned to available AlphaFold models for human HCCS and *P. falciparum* HCCS and HCC_1S. Superposition of these structural models indicated very similar predicted structures for all three orthologs (**Fig. S2**), consistent with their substantial sequence similarity. The AlphaFold models suggest a central β-sheet that packs against an extended α-helix to create a central hydrophobic pocket, with several shorter α-helices predicted to pack around this hydrophobic core (**Fig. 2B and Fig. S2**). This predicted structure differs from a recent structural model for human HCCS generated by Rosetta and co-evolution approaches, which suggested a predominantly α-helical core structure (24). Nevertheless, both models predict that H154 is positioned within the protein core, where this residue is expected to coordinate bound heme (23). Indeed, AlphaFold 3 (33) modeled heme bound within the hydrophobic interior of parasite HCCS in an orientation coordinated by H154 (**Fig. S3**). The AlphaFold models further suggest that conserved H211 is positioned opposite H154 to possibly play a role as a second axial ligand for bound heme (**Fig. 2B and Fig. S3**). Prior mutagenesis studies with human HCCS found that H211 mutants showed minor reductions in heme attachment to cyt *c* that were less severe than H154 mutants (23), suggesting that H211 could contribute to heme binding to HCCS prior to association with apo cyt *c*. Such a role within the HCCS active site may underpin sequence conservation of H211 across phylogenetically disparate HCCS orthologs (**Fig. 2A**).

We noted that AlphaFold 3 generated two distinct models for heme-bound HCCS, differing in the position of a central α-helix that either exposed or occluded the bound heme (**Fig. S3**). In both conformations, a conserved Lys residue (K133) was positioned within 2-4 Å of a heme

propionate, suggesting a stabilizing electrostatic interaction that might underpin the strict conservation of this residue. The position of the central helix also appeared to pivot about a conserved Gly residue (G140), whose inherent conformational freedom may provide a flexible joint to enable rigid-body reorientation of this helix. The equilibrium distribution of these conformations gated by helical rearrangement may be critical for exposing the heme-bound HCCS active site for selective binding to the cyt *c* N-terminus during HCCS-catalyzed hemylation. Incisive tests of these hypotheses will require overcoming technical challenges to HCCS solubilization that have hampered experimental structure determination of this protein.

We next used AlphaFold 3 to model a possible complex between *P. falciparum* HCCS, heme, and the N-terminal 33 residues of cyt *c*, which include the N-terminal α-helix and CXXCH motif critical for recognition and heme attachment by HCCS (23, 34). In the modeled protein complex (**Fig. 2D**), which AlphaFold 3 generated based only on the input amino acid sequences and selecting heme as ligand, the N-terminal α-helix of cyt *c* packs against and perpendicular to one end of the central α-helix of HCCS. This orientation positions the conserved Cys residues of the CXXCH motif proximal to the active site cavity such that the conserved cyt *c* His residue (H19 in human numbering) extends into the HCCS active site and replaces H211 of HCCS in an orientation opposite H154. AlphaFold 3 modeled heme bound within the hydrophobic core of HCCS with the central iron coordinated by H154 of HCCS and the conserved H19 of cyt *c* such that the vinyl groups of heme were positioned proximal to C16 and C18 of cyt *c* (**Fig. 2D**). This model suggests a key intermediate in cyt *c* hemylation in which HCCS-bound heme is positioned by opposing His coordination to facilitate thioether bond formation between the Cys residues of cyt *c* and heme vinyl groups. This model is consistent with prior mechanistic suggestions for

human HCCS maturation of cyt *c* based on biochemical experiments and structural modeling (23, 24, 35).

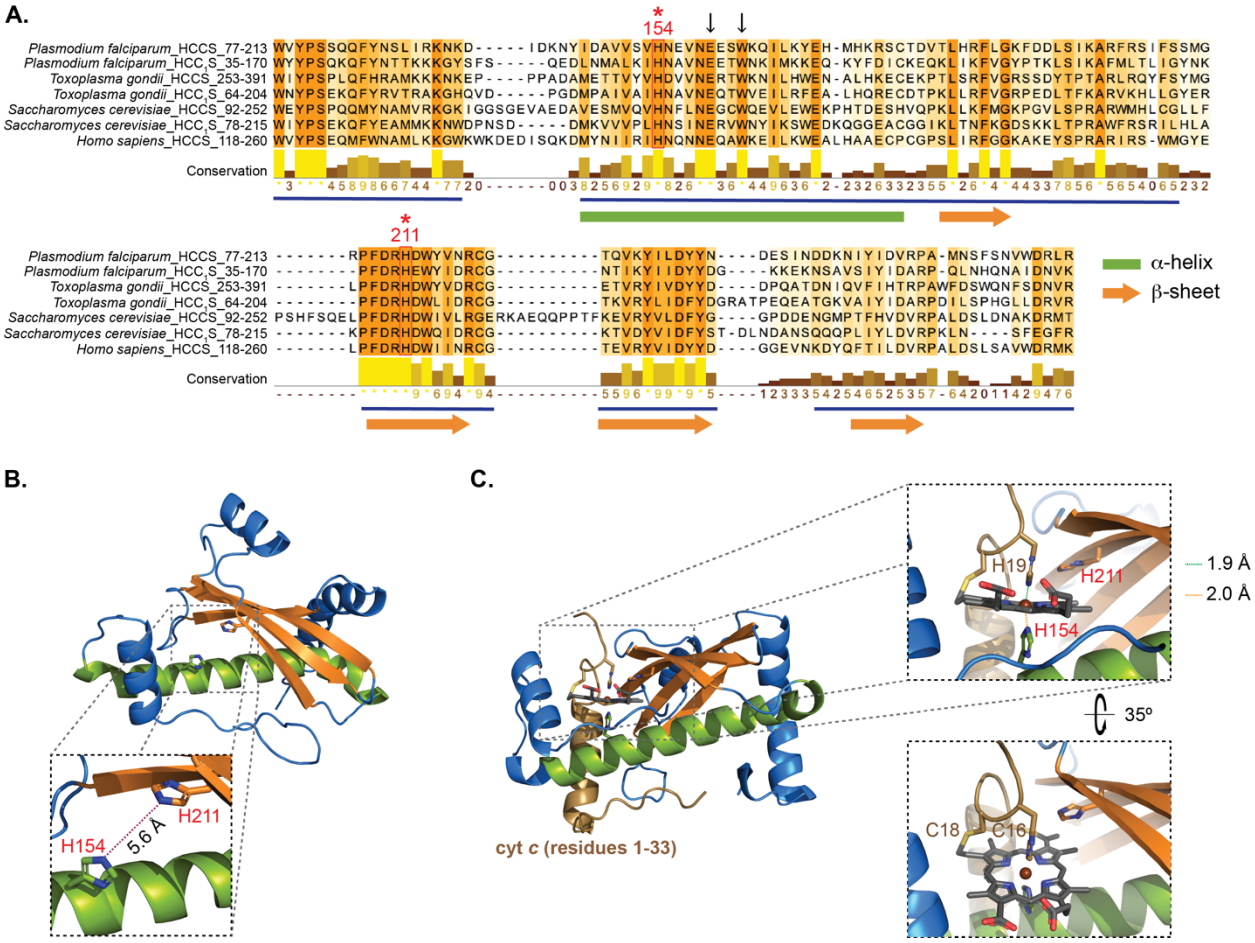

Figure 2. Sequence and structural analysis of HCCS homologs. (A) CLUSTAL Sequence alignment of *P. falciparum* HCCS (77-213) and HCC_1S (35-170) with homologs from *T. gondii* (HCCS: TGME49_293390, 92-252, and HCC_1S: TGME49_314042, 64-204), *S. cerevisiae* (HCCS: CYC3/YAL039C, 92-252; and HCC_1S: CYT2/YKL087C, 78-215), and *H. sapiens* (NP_001116080.1, 118-260). Conservation was measured by JalView with high scores (>5) underlined in blue. Vertical arrows and red asterisks highlight key conserved residues. For simplicity, N-terminal leader sequences are not shown. Residues included in alignments are indicated. (B) AlphaFold model for PfHCCS showing proximity of conserved active-site His residues (H154, green; and H211, orange; human numbering). (C) AlphaFold 3 model of PfHCCS bound to heme and the N-terminal 33 amino acids of *P. falciparum* cyt *c* (Pf3D7_1404100) showing proximity of conserved His residues from HCCS (H154, green) and cyt *c* (H19, brown), using human sequence numbering.

Parasite HCCS and HCC_1S localize to mitochondria. A prior study of GFP-tagged *P. falciparum* HCCS and HCC_1S localized both proteins to the parasite mitochondrion using wide-field fluorescence microscopy (16). To further test this conclusion, we imaged Dd2 parasites episomally expressing HCCS-GFP and HCC_1S-GFP on a spinning disk confocal microscope and evaluated colocalization with MitoTracker Red staining. For both proteins, we observed focal GFP signal that overlaid closely with MitoTracker signal but did not further specify or confirm targeting to the intermembrane space, the expected mitochondrial localization of HCCS proteins (36).

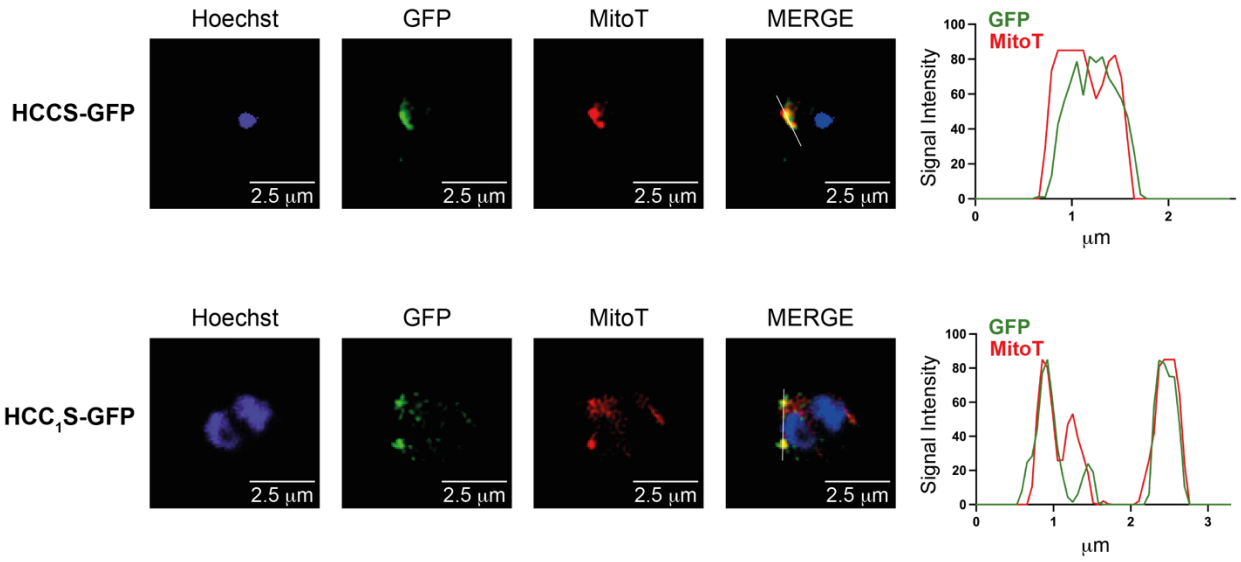

Figure 3. Fluorescence microscopy of live blood-stage *P. falciparum* Dd2 parasites episomally expressing HCCS-GFP and HCC_1S-GFP and stained with 1 nM MitoTracker Red (MitoT) and Hoechst (nucleus). Intensity plots display the overlap in pixel intensity for GFP and MitoTracker Red as a function of distance along the white line in the merged images.

HCC_1S is essential for parasite viability, ETC function, and cyt c_1 biogenesis. Prior genome-wide and targeted knockout studies in *P. falciparum* and *P. berghei* reported that both HCCS and HCC_1S genes were refractory to disruption and thus likely essential (28-30), but neither protein has been directly studied in *Plasmodium*. We first focused on HCC_1S, since our prior heterologous

expression studies in *E. coli* suggested that this protein does not hemylate cyt *c* but were unable to specify a function for this protein in cyt c_1 biogenesis (16). To directly test HCC_1S function in *P. falciparum*, we used CRISPR/Cas9 to edit the HCC_1S gene in Dd2 parasites to encode a C-terminal HA-FLAG epitope tag fusion and the 10x aptamer/TetR-DOZI system for conditional protein expression (37). In this system, protein expression occurs in the presence of the non-toxic small molecule, anhydrotetracycline (aTc) but is repressed upon aTc washout. PCR analysis confirmed correct editing of the HCC_1S gene in transfected parasites (**Fig. S4**).

To evaluate HCC_1S expression and its down-regulation upon aTc washout, we performed western blot (WB) experiments to detect the HA-FLAG epitope tags. In repeated experiments that included mitochondrial isolations, we were unable to detect the endogenously tagged protein, likely reflecting very low expression in blood-stage parasites and/or unusual solubility properties that resisted extraction in Triton X-100 and SDS. To bypass this limitation, we used reverse transcription and quantitative PCR (RT-qPCR) to measure mRNA levels as a proxy for protein expression. The aptamer/TetR-DOZI system was designed to suppress translation by sequestering transcripts in P-bodies (37), and multiple prior studies have revealed a loss of transcript levels in –aTc conditions that suggests transcript degradation (38, 39). By RT-qPCR, we detected a strong reduction in transcript levels (~70%) in -aTc compared to +aTc conditions that indicated robust down-regulation of HCC_1S expression upon aTc washout (**Fig. 4A**). To evaluate the impact of HCC_1S knockdown on parasite growth, we synchronized the tagged parasites and evaluated their growth over 6 days (3 intraerythrocytic cycles) in ±aTc conditions. Parasites grew normally +aTc, but their growth was strongly suppressed after 2 days in -aTc conditions (**Fig. 4A**). By blood smear, we detected wide-spread evidence of parasite death at longer growth times, indicating that HCC_1S function was essential for blood-stage growth.

Prior works have shown that blood-stage parasites can be rescued from defects in the mitochondrial electron transport chain by exogenous addition of the soluble ubiquinone analog, decyl-ubiquinone (dQ) (14-16). HCC_1S knockdown is predicted to impair biogenesis of cyt c_1, which is an integral and essential component of ETC Complex III. We thus predicted that dQ might rescue parasites from lethal loss of HCC_1S (**Fig. 1**). To test this prediction, we supplemented parasite cultures with 15 μM dQ and monitored growth over 8 days ±aTc. We observed that dQ supplementation substantially rescued parasite growth in -aTc conditions (**Fig. 4B**), supporting a key role for HCC_1S in ETC function. Addition of 1 μM proguanil (PRG), which inhibits the secondary pathway for mitochondrial polarization (9, 17), minimally impacted parasite growth in +aTc conditions but negated dQ rescue and strongly impaired parasite growth in –aTc/+dQ conditions, as expected for defective ETC function upon HCC_1S knockdown (**Fig. 4B**). Fluorescence microscopy of parasites grown for 5 days ±aTc/+dQ revealed that 1 μM proguanil specifically resulted in dispersed MitoTracker Red staining in -aTc conditions, which indicates mitochondrial depolarization (**Fig. 4C** and **Fig. S5**) (9, 15, 16). We conclude that HCC_1S knockdown selectively impairs ETC function and sensitizes parasites to mitochondrial depolarization by proguanil, as expected for defective cyt c_1 function.

Impairment of cyt c_1 hemylation may reduce the folding stability and thus detectable levels of cyt c_1 and/or its assembly into Complex III. To test the impact of HCC_1S knockdown on cyt c_1 levels, we tagged the HCC_1S gene with the aptamer/TetR-DOZI system in Dd2 parasites that episomally expressed cyt c_1-GFP (15) and confirmed integration by PCR (**Fig. S6**). Growth assays with synchronized parasites revealed a strong growth impairment in -aTc conditions (**Fig. S7**) that was very similar to the original HCC_1S knockdown line (**Fig. 4A**). We harvested biological triplicate samples after 3 days of growth in ±aTc/+dQ conditions, and fractionated samples by

SDS-PAGE followed by western blot (WB) analysis of cyt c_1-GFP levels. This experiment revealed that HCC_1S knockdown reduced cyt c_1-GFP levels by ~35% but did not impact mitochondrial Hsp60 levels (**Fig. 4D** and **Fig. S8**), supporting a key role for HCC_1S in cyt c_1 maturation and stability. It is possible that the GFP tag may stabilize apo cyt c_1 and thus mask a stronger reduction in cyt c_1 levels upon HCC_1S knockdown.

To test the impact of HCC_1S knockdown on cyt c_1 incorporation into Complex III, we harvested samples after 5 days of growth in ±aTc/+dQ conditions and fractionated them by blue-native PAGE followed by WB analysis. Anti-GFP staining revealed a strong band at ~700 kDa in +aTc conditions (**Fig. 4E** and **Fig. S8**), which is the expected size for Complex III dimer and consistent with recent BN-PAGE detections of Complex III in *P. falciparum* and *Toxoplasma gondii* (40-43). HCC_1S knockdown in -aTc conditions, however, reduced the intensity of the 700 kDa band by ≥65%, suggesting a substantial defect in cyt c_1 assembly into Complex III. We conclude that HCC_1S is essential for cyt c_1 biogenesis and assembly into ETC Complex III.

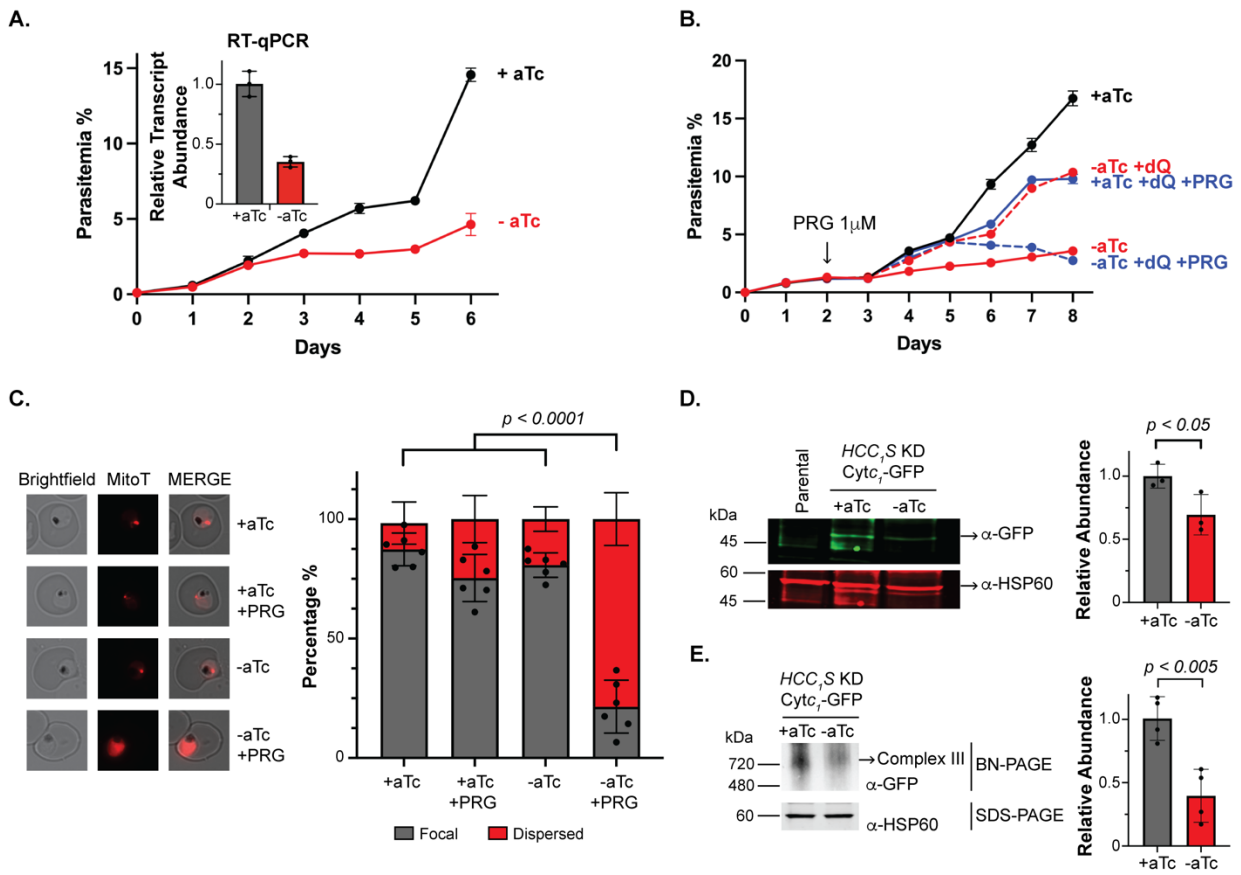

Figure 4. Functional impacts of HCC_1S knockdown. (A) Synchronous growth assay of Dd2 parasites tagged with the aptamer/TetR-DOZI cassette with normal expression (+aTc) or inducible knockdown (-aTc) of HCC_1S expression. Inset: RT-qPCR analysis of HCC_1S transcript levels (normalized to I5P, Pf3D7_0802500, and ADSL, Pf3D7_0206700) in biological triplicate samples cultured 4 days ±aTc in 15 μM decyl-ubiquinone (dQ). (B) Synchronous growth assay of HCC_1S knockdown parasites cultured ±aTc, ±15 μM dQ, and ±1 μM proguanil (PRG, added day 2). Data points are the average ±SD of biological triplicates. (C) Fluorescence microscopy images of live HCC_1S knockdown parasites cultured 5 days in 15 μM dQ, ±aTc, and ±1 μM proguanil and stained with 1 nM MitoTracker Red (MitoT). Thirty parasites were imaged in each of 6 biological replicates to score MitoT staining as focal or dispersed and calculate the percentage of the total population in each condition with the indicated mitochondrial phenotype (average ±SD, *p* value from two-tailed unpaired *t*-test). (D) SDS-PAGE/WB analysis of cyt c_1-GFP expression levels in HCC_1S knockdown parasites cultured 3 days ±aTc/+dQ. Blot was probed with α-GFP and α-Hsp60 antibodies. Band intensities were quantified by densitometry, and the average normalized GFP:Hsp60 signal ±SD based on biological triplicate samples was plotted for ±aTc conditions (*p* value from two-tailed unpaired *t*-test). (E) Blue native-PAGE/WB analysis of cyt c_1-GFP and SDS-PAGE/WB analysis of HSP60 expression levels in HCC_1S knockdown parasites cultured 5 days ±aTc/+dQ. 20 μg of total protein from mitochondrial lysates were loaded for each lane. Blots were probed with α-GFP or α-HSP60 antibodies, with band intensities quantified by densitometry. The average normalized GFP intensity ±SD from biological replicates was plotted for ±aTc conditions. WB images from biological replicates and uncropped blots for (D) and (E) are shown in **Fig. S8** and **Fig. S9**, respectively.

Loss of HCCS sensitizes parasites to mitochondrial depolarization by proguanil. To directly test HCCS function in blood-stage *P. falciparum*, we used a similar CRISPR/Cas9 strategy to tag the HCCS gene in Dd2 parasites to encode a HA-FLAG fusion tag and the aptamer/TetR-DOZI system for conditional knockdown. We used genomic PCR to confirm successful integration and gene editing in clonal parasites (**Fig. S4**). As with HCC_1S, we were unable to detect the HA-FLAG-tagged HCCS by WB analysis, suggesting similar low expression. However, RT-qPCR analysis of transcript levels after 3 days of synchronous growth ±aTc revealed a ~70% reduction in HCCS mRNA levels that was similar to that observed for HCC_1S (**Fig. 5A**). Synchronous growth assays in ±aTc conditions revealed a modest growth defect in -aTc conditions in the third cycle that was less severe than observed for HCC_1S but suggested possible defects in ETC function. To test if this more modest phenotype was specific to HCCS knockdown in Dd2, we also tagged HCCS for knockdown in NF54 parasites and observed a similar phenotype (**Fig. S10**).

Addition of 1 μM proguanil had little or no impact on parasite growth +aTc but resulted in a stringent growth defect and parasite death in -aTc conditions (**Fig. 5B**). This observation suggests that HCCS knockdown results in a critical defect in proton translocation by Complex III and/or IV that is only unmasked in the presence of proguanil and inhibition of the secondary mechanism for mitochondrial polarization. Analysis by fluorescence microscopy, which revealed that proguanil selectively impaired mitochondrial accumulation of MitoTracker Red in -aTc conditions (**Fig. 5C** and **Fig. S5**), provided further support for this conclusion. Based on our prior observation that *P. falciparum* HCCS hemylates cyt *c* in heterologous expression studies in *E. coli* (16), we propose that HCCS knockdown in parasites impairs holo-cyt *c* biogenesis and reduces proton pumping by ETC Complex III and/or IV that sensitizes parasites to lethal mitochondrial depolarization by

proguanil (**Fig. 1**). We further explore the phenotypic differences between HCC_1S and HCCS knockdowns in the Discussion section below.

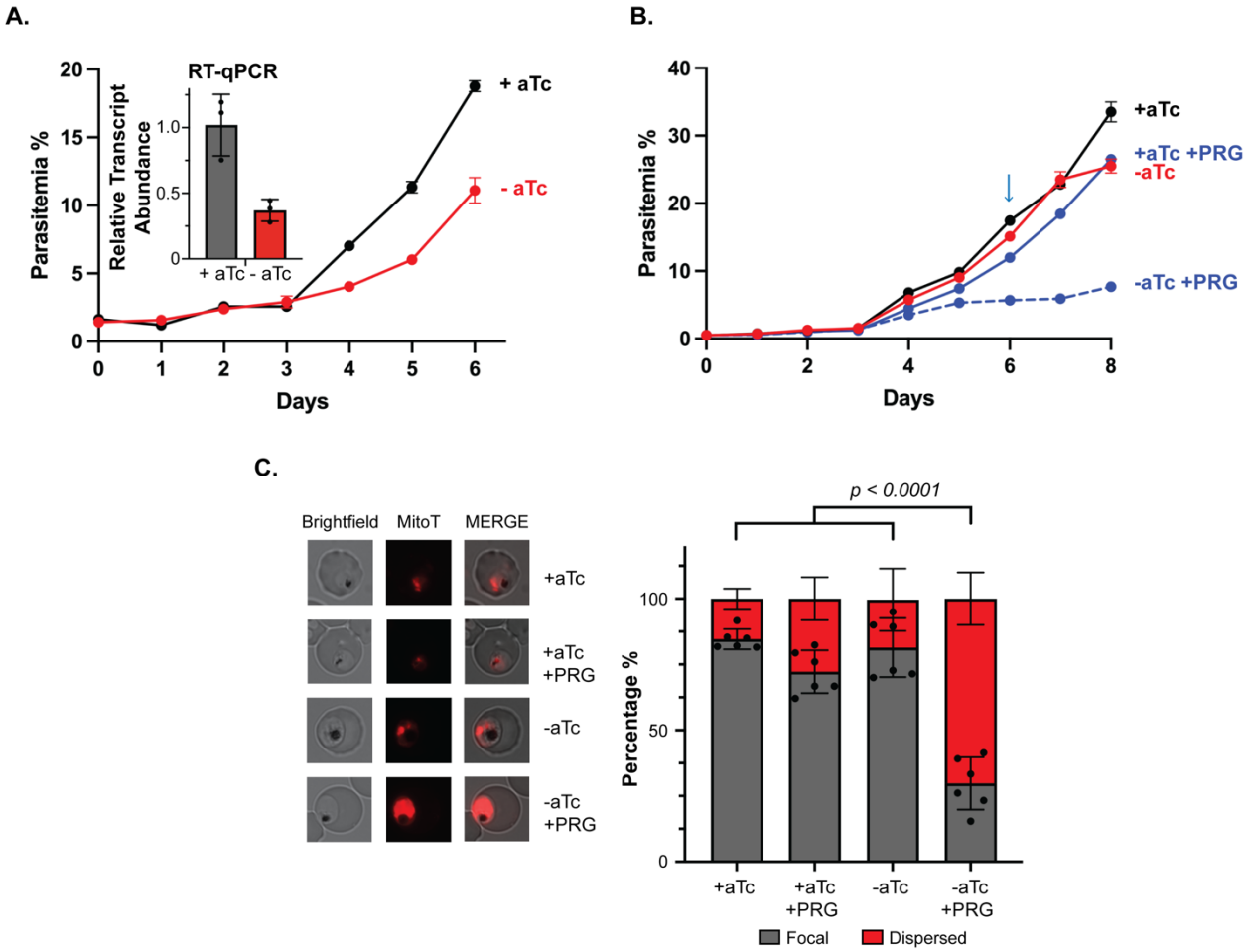

Figure 5. Functional impacts of HCCS knockdown. (A) Synchronous growth assay of Dd2 parasites (clone 1P10) tagged with the aptamer/TetR-DOZI cassette with normal expression (+aTc) or inducible knockdown (-aTc) of HCCS expression. Inset: RT-qPCR analysis of HCCS transcript levels (normalized to I5P and ADSL) in biological triplicates of synchronous parasites cultured 4 days ±aTc. (B) Synchronous growth assay of HCCS knockdown parasites cultured ±aTc and ±1 μM proguanil (PRG). All growth assay data points are the average ±SD of biological triplicates. Arrow indicates culture splits. (C) Fluorescence microscopy images of live HCCS knockdown parasites cultured 5 days ±aTc and ±1 μM proguanil and stained with 1 nM MitoTracker Red (MitoT). Thirty parasites were imaged in each of 6 biological replicates to score MitoT staining as focal or dispersed and calculate the percentage of the total population in each condition displaying the indicated mitochondrial phenotype (average ±SD). Significance was analyzed by two-tailed unpaired *t*-test to determine the indicated *p* values.

***P. falciparum* HCCS and HCC_1S have distinct functional specificities.** Targeted gene knockout studies in *P. berghei* (30), prior biochemical experiments (16), and observations in this study of parasite growth defects upon knockdown of HCC_1S or HCCS (exacerbated by non-lethal proguanil) suggest essential and non-redundant functions and specificities for these proteins. To further test this conclusion, we tagged the HCCS or HCC_1S gene for conditional knockdown in the prior Dd2 parasite lines that episomally expressed HCCS-GFP or HCC_1S-GFP (16) and confirmed correct integration by genomic PCR (**Fig. S6 and Fig. S11**). Synchronous growth assays revealed that parasites episomally expressing HCC_1S-GFP were insensitive to knockdown of endogenous HCC_1S and grew similarly in ±aTc conditions (**Fig. 6A**), as expected if episomal HCC_1S-GFP functionally replaced the endogenous HCC_1S. However, parasites episomally expressing HCCS-GFP displayed a severe growth defect upon HCC_1S knockdown in -aTc conditions that was rescued by dQ (**Fig. 6B**), suggesting that HCCS is unable to functionally replace HCC_1S. We observed the opposite pattern of rescue for loss of HCCS. Knockdown of endogenous HCCS resulted in no detectable growth impairment in parasites expressing HCCS-GFP (**Fig. 6C**) but a measurable growth defect in parasites expressing HCC_1S-GFP (**Fig. 6D)** These observations support our conclusion that HCCS and HCC_1S have distinct specificities for hemylation of cyt *c* and c_1 that underpin non-redundant and critical functions.

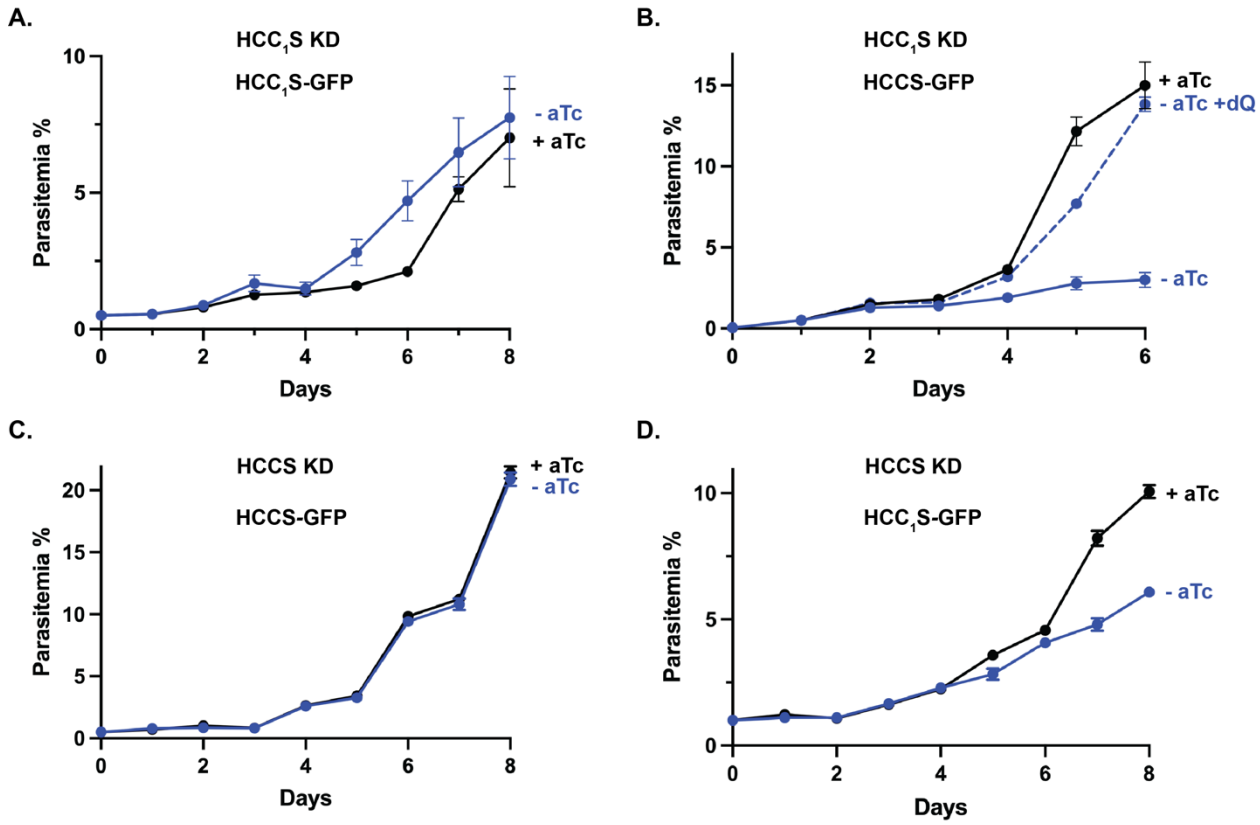

Figure 6. *P. falciparum* HCCS and HCC_1S have non-redundant functions. Synchronous growth assays of HCC_1S knockdown parasites episomally expressing HCC_1S-GFP (A) or HCCS-GFP (B) or HCCS knockdown parasites episomally expressing HCCS-GFP (C) or HCC_1S-GFP (D) and cultured in ±aTc and ±dQ (15 µM) conditions. All growth assay data points are the average ±SD of biological triplicate samples.

DISCUSSION

The maturation and function of heme-bound cyt *c* and cyt c_1 are central to mitochondrial electron transport chain activity in malaria parasites, especially respiratory Complexes III and IV (**Fig. 1**). Complex III is the molecular target of atovaquone (8) and has received considerable attention in the discovery and development of new antimalarial drugs (10, 12), especially as parasites that harbor atovaquone-resistant mutations are unable to complete mosquito-stage development and transmit to new hosts (44, 45). Prior work has also highlighted effective strategies to target parasites via Complex III during mosquito infection (11). These studies are nearly all based on targeting cyt *b* of Complex III, and few strategies have been identified to interfere with other essential ETC factors and functions. Recent efforts dissected the essential roles of cyt *c* and c_1 for parasite ETC activity (16), but it is unclear how these protein functions might be directly targeted. In the present work, we identified critical independent functions for HCCS and HCC_1S, required for covalent attachment of heme to cyt *c* and c_1. This work lays a foundation for deeper structural and mechanistic studies to unravel differences within the heme-binding pockets of the human and parasite HCCS enzymes that can underpin selective therapeutic targeting of the *P. falciparum* ETC.

Functional differences between *P. falciparum* HCCS and HCC_1S. This study, in combination with prior functional tests based on heterologous reconstitution in *E. coli* (16), unveiled separate key functions for parasite HCCS and HCC_1S in maturation of cyt *c* and c_1, respectively (**Fig. 7**). Knockdown of HCC_1S resulted in impaired cyt c_1 biogenesis and incorporation into Complex III, lethal ETC dysfunction that stringently limited growth and could not be rescued by HCCS over-expression, and strong sensitivity to mitochondrial depolarization in the presence of proguanil. In

comparison, HCCS knockdown caused a modest reduction in parasite growth that required combinatorial treatment with proguanil to stringently kill parasites via mitochondrial depolarization.

The strong growth defect due to loss of HCC_1S phenocopies direct knockdown of cyt c_1 (16) and underscores the tight dependence of ETC function and parasite viability on cyt c_1 expression and heme-dependent maturation. This stringent coupling to cyt c_1 may reflect both the direct function of cyt c_1 in mediating critical electron transfer from the Rieske Fe-S protein to cyt *c* (46) and a secondary structural role played by cyt c_1 in the assembly and integrity of Complex III (47), both of which are likely impaired by loss of HCC_1S (**Fig. 7**). Indeed, our data provide direct evidence that HCC_1S knockdown results in defective cyt c_1 incorporation into Complex III (**Fig. 4E**). Prior work in yeast also highlighted that hemylation of cyt c_1 by HCC_1S is coupled to mitochondrial import and N-terminal processing (48). Import and processing of cyt c_1 is sparsely studied in apicomplexan parasites. Nevertheless, recent work in *Toxoplasma* identified that the cyt c_1 leader sequence that is cleaved upon mitochondrial import is incorporated into ATP synthase as a stable structural sub-unit (41, 49). It is not clear if this sub-unit is required for assembly and/or function of ATP synthase nor if this feature is conserved in *Plasmodium* parasites. Proteomic profiling of ATP synthase composition in *P. falciparum* did not report this cyt c_1-derived subunit (40), although associations between cyt c_1 and ATP synthase have been detected in blood-stage parasites (50). Nevertheless, this observation in *T. gondii* suggests an additional (and elegant) biochemical mechanism to couple cyt c_1 import, hemylation, and maturation in apicomplexan parasites to broader assembly and function of the mitochondrial ETC beyond Complex III.

The more modest growth phenotype upon knockdown of HCCS compared to HCC_1S, despite similar reductions in transcript abundance, is somewhat puzzling and may have multiple

underpinnings. Cyt *c* function, which depends on heme attachment, is essential for ETC function and parasite viability (16). The mild phenotype for HCCS knockdown thus contrasts with the lethal phenotype for cyt *c* knockdown, the strong expectation of HCCS essentiality based on prior knockout studies (28-30), and the selective ability of HCCS (and not HCC_1S) to hemylate cyt *c* in heterologous studies in *E. coli* (16). The first explanation we considered is that HCCS knockdown was insufficiently stringent such that residual expression was enough to support cyt *c* hemylation and attenuate the phenotypic severity of partial knockdown. However, HCCS knockdown sensitizes parasites to a much stronger, lethal phenotype when combined with 1 μM proguanil. This observation suggests a critical defect in proton pumping by Complexes III and/or IV due to HCCS knockdown, despite modest growth inhibition by itself, which can explain the synergistic lethality with proguanil which blocks the secondary pathway for mitochondrial polarization (**Figs. 1 and 7**).

Based on these observations, we favor an alternative model that HCCS knockdown in our current system impairs cyt *c* hemylation sufficiently to interfere with electron transport between Complexes III and IV but without substantially impairing oxidative recycling of ubiquinone by Complex III. A corollary of this model is that cyt *c*-mediated electron transport to Complex IV and concomitant proton pumping may be more tightly coupled to cyt *c* function than ubiquinone recycling by Complex III. This model predicts that a more stringent knockdown of HCCS, which might be achieved by adding a 5' aptamer to the current 10x aptamers on the 3' end of the HCCS gene, will impair ubiquinone recycling and result in a lethal growth phenotype that matches direct knockdown of cyt *c* and can be rescued by decyl-ubiquinone (16). We are currently testing this prediction.

Implications for evolution of *P. falciparum* HCCS and HCC_1S. Cyt *c* and c_1 are retained by nearly all aerobic eukaryotes with a mitochondrion (20, 21, 51). Nature has evolved at least three distinct biochemical systems for *c*-type cytochrome hemylation, two of which are multi-protein systems that are unrelated evolutionarily to the single-protein HCCS system (18, 19, 52). HCCS and/or HCC_1S proteins are broadly present in eukaryotes, including opisthokonts, alveolates, and amoebazoa (52). This broad retention across phylogenetically divergent organisms suggests that separate HCCS and HCC_1S enzymes are ancient features of many eukaryotes. Within these clades that contain an HCCS homolog, metazoa and amoebozoa retain a single homolog (**Fig. S1**) that appears to bifunctionally hemylate both cyt *c* and c_1 (19, 25). For these organisms, low-level promiscuous hemylation of cyt c_1 (in addition to the cognate cyt *c* substrate) was presumably enhanced in an ancestral organism such that a separate HCC_1S enzyme became redundant and was lost (19, 23). Evidence for this model is provided by yeast, in which HCCS hemylates cyt *c* and less efficiently cyt c_1 (25). As previously noted (52), the evolutionary origin of HCCS is unclear and remains a future challenge to understand. Indeed, our structural similarity searches of the RCSB Protein Data Bank with the AlphaFold-predicted *P. falciparum* HCCS structure using the Dali server (53) failed to identify substantial similarity to known protein structures.

Based on our studies, *P. falciparum* HCCS and HCC_1S show no evidence for functional redundancy or promiscuity, and both appear to be essential. This scenario contrasts with the related apicomplexan parasite *Toxoplasma gondii*, in which only the HCCS homolog appears to be essential for tachyzoite survival and shows evidence of hemylating both cyt *c* and c_1, despite retention of an HCC_1S paralog (27). Thus, the function, retention, and essentiality of HCCS and HCC_1S homologs may be idiosyncratically tuned during evolution of different organisms depending on their unique cellular pressures for growth and survival. These functional differences

may also involve additional cellular factors that influence observed specificities in vivo. Broader and deeper functional studies of these enzymes in differing organisms will facilitate understanding of the gain and loss of activities that underpin evolution of this enzymatic activity central to eukaryotic respiration.

Source of heme for HCCS and HCC_1S. *Plasmodium* parasites require heme as a metabolic cofactor for incorporation into mitochondrial cytochromes *b* and c_1 in Complex III, cyt *c*, and cytochrome a/a_3 in Complex IV (2-4). Parasites retain a complete biosynthesis pathway to make heme in the mitochondrion, but this pathway is dispensable for parasites during blood-stage growth and is only required during mosquito- and liver-stage growth (54-59). This observation implies that parasites can scavenge host-derived heme, although possible mechanisms for mobilizing labile heme released in the food vacuole during hemoglobin digestion and trafficking it to the mitochondrion remain undefined. HCCS and HCC_1S function on the outer leaflet of the mitochondrial inner membrane (36) and must bind heme for subsequent attachment to cyt *c* and c_1. Although proteomic studies in human cells suggest that the terminal heme synthesis enzyme, ferrochelatase, associates with other heme metabolism proteins at the mitochondrial inner membrane that may include or facilitate heme acquisition by HCCS (60, 61), parasite mechanisms for acquisition of biosynthetic or scavenged heme by HCCS and HCC_1S are unknown. Our current study does not provide an answer to this question but lays a foundation for defining key interactions by these enzymes in *P. falciparum*, either through immunoprecipitation or proximity biotinylation coupled to tandem mass spectrometry, that can illuminate the heme-trafficking pathways that support biogenesis of heme-bound cyt *c* and c_1.

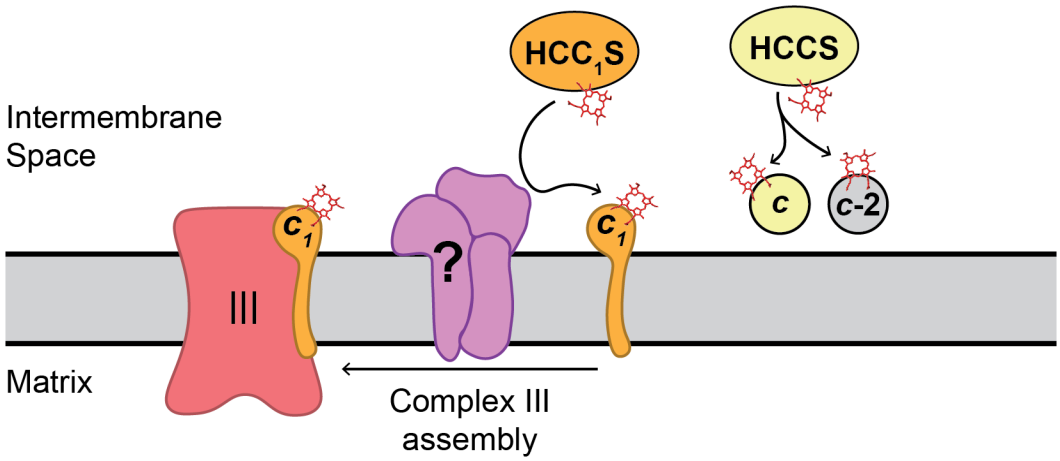

Figure 7. Schematic model for functional specificities of *P. falciparum* HCCS and HCC_1S. The question mark indicates uncertainty in the mechanism of cyt c_1 assembly into Complex III.

METHODS

Cloning. Creation of pTEOE plasmids encoding HCCS-GFP and HCC_1S-GFP was previously described (16). To tag HCCS and HCC_1S for inducible knockdown, guide RNA sequences corresponding to TAACAAAAATTGTGAAAAAT and GCAAATGTGCAACAAACAAT (HCCS) and TTATTTATATAAAGATTTGT (HCC_1S) were cloned into the pAIO CRISPR/Cas9 vector (62) using ligation-independent methods (primers HCCSgRNA1F, HCCSgRNA1R, HCCSgRNA2F, HCCSgRNA2R, HCC1SgRNA1F and HCC1SgRNA1R) by the Mutation Generation & Detection Core at the University of Utah. Donor repair plasmids for each gene were creating using assembly PCR to create a fused sequence containing a 3' UTR homology region (HR) separated by an AflII site from a 5' homology region that contained the 3' end of the coding sequence (without stop codon) for each gene. This fused insert was then cloned into the pMG75 (37) plasmid using AscI/AatII cloning sites and ligation-independent methods and confirmed by Sanger sequencing. Donor plasmids to tag each gene were cloned from genomic DNA using the

following primer sets: HCCS (3' HR: primers 51/52, 5' HR: primers 53/54) and HCC_1S (3' HR: primers 55/56, 5' HR: primers 57/58). Primer sequences are given in Table S1.

Parasite Culturing and Transfection. Experiments in this study were performed using *Plasmodium falciparum* Dd2 (63) and NF54 (64) parasites, whose identities were confirmed based on expected drug sensitivities and resistance. Parasites were *Mycoplasma*-free by PCR test. Dd2 parasites stably transfected with a pTEOE episome (59) encoding HCCS-GFP or HCC_1S-GFP were available from a previously reported study (16) and cultured in 5 nM WR99210.

Parasites were cultured as previously described (16, 39), using Roswell Park Memorial Institute medium (RPMI-1640, Thermo Fisher 23400021) supplemented with 205 g/L AlbuMAX I Lipid-Rich BSA (Thermo Fisher 11020039), 15 mg/L hypoxanthine (Sigma H9636), 110 ml/L sodium pyruvate (Sigma P5280), 1.19 g/L HEPES (Sigma H4034), 2052 g/L sodium bicarbonate (Sigma S5761), 2 g/L glucose (Sigma G7021), and 10 mg/L gentamicin (Invitrogen 15750060). Parasites were grown at 2% hematocrit in human red blood cells obtained from the University of Utah Hospital blood bank, at 37˚C, and at 5% O_2, 5% CO_2, and 90% N_2. Parasite-infected cultures were transfected in 1x cytomix (65) containing 50-100 µg midi-prep DNA by electroporation in 0.2 cm cuvettes using a Bio-Rad Gene Pulser Xcell system (0.31 kV, 925 µF). Transgenic parasites were selected based on plasmid resistance (blasticidin-S-deaminase) to 6 µM blasticidin-S (Gold Biotechnology B-800-100). Transgenic parasites modified with the aptamer/TetR-DOZI system or pTEOE episomes were cultured in 0.5-1 µM anhydrotetracycline (aTc, Cayman Chemicals 10009542) or 5 nM WR99210 (Jacobus Pharmaceuticals), respectively. Genetically modified parasites were genotyped by PCR. For growth assays with decyl-ubiquinone (dQ, Caymen Chemicals 55486005) and/or proguanil (Sigma 637321), the growth medium was supplemented with 15 µM dQ (≤0.3 % DMSO) and/or 1 µM proguanil (≤0.3 % DMSO).

For CRISPR/Cas9-based genome-editing experiments to tag HCCS (PF3D7_1224600) and HCC_1S (PF3D7_1203600) to encode a C-terminal HA-FLAG epitope tag and the 10X aptamer/TetR-DOZI system for aTc-dependent expression (37), Dd2 or NF54 parasites were transfected in duplicate with 50 µg each of the linearized pMG74 donor plasmid (with gene-specific homology arms) and pAIO plasmid (62) (encoding Cas9 and gene-specific gRNA). Transfected parasites recovered for 48 hours in drug-free media and then were selected with 0.5 µM aTc and 6 µM blasticidin-S. Polyclonal parasites that returned from transfection were genotyped with primer sets 77_P1/52_P2 and 77_P1/83_P3 (HCCS) and 86_P1/58_P2 and 86_P1/57_P3 (HCC_1S) to test for unmodified locus and successful integration, respectively. Polyclonal parasites that PCR analysis indicated were fully integrated without unmodified locus were used without cloning. Otherwise, clonal parasite integrants were obtained by limiting dilution. The Dd2 lines with HCC_1S tagged for KD at its endogenous locus and episomally expressing cyt c_1-GFP was created by first transfecting Dd2 parasites with cyt c_1-GFP/pTEOE (selection with WR99210) and then transfecting with pAIO CRISPR/Cas9 and pMG75/donor repair plasmids to tag the HCC_1S gene for knockdown (selection with blasticidin-S and aTc). Successful integration was confirmed by genotyping PCR as above. A similar strategy was used to tag HCCS or HCC_1S for KD at its endogenous locus in DD2 parasites that episomally expressed HCCS-GFP or HCC_1S-GFP and were previously reported (16).

Parasite Growth Assays. For synchronous growth assays, asynchronous parasite cultures were treated with 5% D-sorbitol (Sigma S7900) for 10 minutes to produce ring-stage parasites. Sorbitol-treated cultures were then washed three times with RPMI media lacking aTc and divided into two equal parts before supplementing one part with 0.5 µM aTc. Parasites were diluted to 0.5% parasitemia ±aTc and allowed to grow over several days with daily media changes in biological

triplicate samples. Parasitemia was monitored daily by flow cytometry by diluting 10 µL of each resuspended parasite culture well from each replicate into 200 µL of 1.0 µg/mL acridine orange (Invitrogen A3568) in phosphate buffered saline (PBS) pH 7.5 and analysis on a BD FACSCelesta system monitoring SSC-A, FSC-A, PE-A, FITC-A and PerCP-Cy5-5A channels. Parasitemia values are the average ± standard deviation of biological replicates using GraphPad Prism 9.0.

RT-qPCR Analyses. Biological replicate cultures of HCCS or HCC_1S knockdown Dd2 parasites were synchronized in 5% D sorbitol and grown for 72 hours in +aTc or -aTc/+dQ conditions prior to harvest. Four mL cultures at ~10% parasitemia were harvested by centrifugation (2000 rpm for 3 min in a Beckman Coulter Allegra 25R table-top centrifuge) and stored at -20˚C until use. Total RNA was isolated from frozen pellets and washed using a modified Trizol (Invitrogen) extraction protocol, as previously described (39). Washed and dried RNA pellets were resuspended in RNAse-free water, quantified by NanoDrop Spectrophotometer, and used immediately or stored at -80˚C. One µg of RNA was DNAse-treated and reverse-transcribed using Superscript IV kit (Invitrogen) with the addition of 1 µM gene-specific reverse primers HCCSqR1, HCC_1SqR1, GFPqR1, I5PqR1, and ADSLqR1. Subsequent cDNA was analyzed in technical triplicate through quantitative PCR using SYBR Green fluorescent probe with ROX (Invitrogen) in a QuantStudio 7 qPCR instrument (Applied Biosystems). C_p values for each target gene (primers HCCS_qF1, HCCS_qR1, HCC_1S_qF1, and HCC_1S_qR1) were normalized to average C_p values of the nuclear I5P gene (PF3D7_0802500, I5P_qF1 and I5P_qR1) and ADSL gene (Pf3D7_0206700, ADSL_qF1 and ADSL_qR1), then used to calculate relative RNA abundance values for each culture condition ±aTc, with normalization of the +aTc sample to a value of 1. Data is reported as the average ± SD of ≥3 biological replicates for each condition. All primer sequences are given in Table S1.

Mitochondrial Isolation. Biological replicate 60 mL cultures of HCC_1S KD Dd2 parasites were harvested at 15-18% parasitemia and treated with 0.05% saponin (Sigma 84510) in PBS (pH 8.0), incubated for 5 min at ambient temperature, and centrifuged at 4,000 rpm for 30 min at 4ºC. Isolated parasite-containing pellets were washed twice with PBS pH 8.0 and stored at -80˚C until use. Parasite pellets were thawed on ice and resuspended with MEST buffer (20 mM Tris-HCl pH 7.4, 250 mM D-sorbitol, 1 mM EDTA pH 8.0, and EDTA-free protease inhibitor cocktail (Thermo Fisher J61852.XF). Parasites were lysed by 10 passages through a syringe fitted with a 25-gauge needle and 20 passages with a 27-gauge needle. The cellular debris and unlysed parasites were pelleted twice by cold centrifugation at 6,000 x *g* for 10 min at 4ºC. The supernatant was centrifuged 15 min. at 17,000 x *g* at 4ºC to recover the crude mitochondrial fraction in the pellet. Total protein from the mitochondrial fraction was quantified using the Lowry method (66).

SDS/Blue-Native PAGE and Western Blot Analyses. To evaluate expression levels of cyt c_1-GFP in the HCC_1S KD line ±aTc, biological replicate cultures of parasites were synchronized with 5% D-sorbitol to rings, grown for 72 hours +aTc or -aTc/+dQ, harvested as second-cycle trophozoites and schizonts, processed as described above to isolate mitochondria, and then analyzed by SDS-PAGE or blue native (BN)-PAGE.

For SDS-PAGE, 50 µg of mitochondrial protein was heated in 1X SDS sample buffer containing 5% fresh β-mercaptoethanol for 5 min. at 65˚C and loaded onto 12% polyacrylamide gels, fractionated by gel electrophoresis, and transferred to nitrocellulose membrane, as previously described (15, 16). Membranes were blocked at room temperature for 1 hour in 5% skim milk/PBS and probed overnight at 4˚C with 1:1000 dilutions of rabbit anti-HSP60 (Novus NBP2-12734) and goat anti-GFP (Antibodies.com A121560) antibodies. Membranes were washed 3 times in TBS buffer supplemented with 0.1% TWEEN-20 (Millipore P1379), probed with 1:5,000 dilutions of

donkey anti-rabbit IRDye680 (Licor 926-68023) and donkey anti-goat IRDye800CW (Licor 926-32214) 2˚ antibodies in TBST buffer, washed 3 times in TBST buffer, and imaged on a Licor Odyssey CLx imager. Band intensities were quantified by densitometry using ImageJ and analyzed by GraphPad Prism 9.0.

For BN-PAGE, 20 µg of mitochondrial protein was mixed with 1X Native-PAGE sample buffer (Invitrogen BN2003) supplemented with 1% digitonin and incubated on ice for 15 min. The sample was centrifuged at 17,000 x g for 10 min., and 20 µL of the supernatant was loaded and run on a NativePAGE 4-16% Bis-Tris gel (Invitrogen BN1002BOX) and transferred to PVDF membrane (pre-wetted in 70% methanol). The membrane was destained in 70% methanol and then washed, blocked, probed with goat anti-GFP 1˚ antibody, and washed as above. The membrane was then probed with a 1:5,000 dilution of rabbit anti-goat-HRP 2˚ antibody (Santa Cruz Biotechnology sc-2768), washed, developed using the SuperSignal West Pico PLUS enhanced chemiluminescence reagent (Thermo Fisher 34577), and imaged on an Invitrogen/Thermo Fisher iBright 1500 imager.

Fluorescence Microscopy. For mitochondrial depolarization experiments with HCCS and HCC_1S knockdown parasites, cultures were synchronized with 5% D-sorbitol, cultured +aTc or -aTc/+dQ for 120 hours before addition of 1 µM proguanil for 4 hours and 1 nM MitoTracker Red for 30 minutes, and imaged as third-cycle trophozoites/schizonts. 30 total parasites for each condition across 4 independent experiments were scored for focal or dispersed MitoTracker signal. Images were taken on DIC/brightfield, DAPI, and RFP channels using an EVOS M5000 imaging system. For Dd2 parasites episomally expressing HCC_1S-GFP or HCCS-GFP, cultures were incubated with 1 nM MitoTracker Red and imaged on DAPI, GFP, and RFP channels using a Nikon Ring

TIRF/Spinning Disk Confocal microscope. Images were processed using ImageJ with all brightness/contrast adjustments made on a linear scale.

Alignment and Phylogenetic Analyses. The protein sequences for parasite HCCS (Pf3D7_1224600) and HCC_1S (Pf3D7_1203600) were analyzed by PSI-BLAST (67) to identify orthologs in representative species of distinct organisms. Sequences were aligned by CLUSTAL Omega (68) and analyzed using Jalview (69). The multisequence alignment was uploaded to the IQ-TREE webserver (http://iqtree.cibiv.univie.ac.at) with ultrafast bootstrap analysis. The resulting maximum likelihood phylogenetic tree from 1000 bootstrap alignments was analyzed using FigTree (http://tree.bio.ed.ac.uk/software/figtree/).

Structural Modeling. Structural models for human HCCS and *P. falciparum* HCCS and HCC_1S were obtained from the AlphaFold Protein Structure Database (https://alphafold.ebi.ac.uk) (70). Structural models for parasite HCCS bound to heme without or with the N-terminal 33 residues of *P. falciparum* cyt c (PF3D7_1404100) were generated using AlphaFold 3 (33). Protein models were visualized and analyzed using PyMOL (71).

SUPPORTING INFORMATION. Supporting figures S1-S12 and Table S1 (PDF)

ACKNOWLEDGMENTS. We thank Chris Hill, Robert Kranz, Tyler Starr, Henry Wienkers, and Dennis Winge and members of the Sigala lab for helpful discussions. This work was supported by NIH grant R35GM133764 (PAS) and a Burroughs Wellcome Fund Career Award at the Scientific Interface (PAS). PAS is a Pew Biomedical Scholar, supported by The Pew Charitable Trusts. DNA synthesis and sequencing, fluorescence microscopy, creation of CRISPR/Cas9 reagents, and flow cytometry were performed using core facilities at the University of Utah and the Center for Iron and Heme Disorders.

REFERENCES

1. WHO. World Malaria Report. Geneva, Switzerland: 2023.

2. Sigala PA, Goldberg DE. The peculiarities and paradoxes of *Plasmodium* heme metabolism. Annu Rev Microbiol. **2014**;68:259-78. Epub 20140616. doi: 10.1146/annurev-micro-091313-103537. PubMed PMID: 25002093; PMCID: PMID 25002093.

3. van Dooren GG, Kennedy AT, McFadden GI. The use and abuse of heme in apicomplexan parasites. Antioxid Redox Signal. **2012**;17(4):634-56. Epub 20120316. doi: 10.1089/ars.2012.4539. PubMed PMID: 22320355.

4. Kloehn J, Harding CR, Soldati-Favre D. Supply and demand-heme synthesis, salvage and utilization by Apicomplexa. FEBS J. **2021**;288(2):382-404. Epub 20200623. doi: 10.1111/febs.15445. PubMed PMID: 32530125.

5. Francis SE, Sullivan DJ, Jr., Goldberg DE. Hemoglobin metabolism in the malaria parasite *Plasmodium falciparum*. Annu Rev Microbiol. **1997**;51:97-123. doi: 10.1146/annurev.micro.51.1.97. PubMed PMID: 9343345; PMCID: PMID 9343345.

6. Blasco B, Leroy D, Fidock DA. Antimalarial drug resistance: linking *Plasmodium falciparum* parasite biology to the clinic. Nat Med. **2017**;23(8):917-28. Epub 2017/08/05. doi: 10.1038/nm.4381. PubMed PMID: 28777791; PMCID: PMC5747363.

7. Delves M, Plouffe D, Scheurer C, Meister S, Wittlin S, Winzeler EA, Sinden RE, Leroy D. The activities of current antimalarial drugs on the life cycle stages of *Plasmodium*: a comparative study with human and rodent parasites. PLoS Med. **2012**;9(2):e1001169. Epub 20120221. doi: 10.1371/journal.pmed.1001169. PubMed PMID: 22363211; PMCID: PMC3283556.

8. Fry M, Pudney M. Site of action of the antimalarial hydroxynaphthoquinone, 2-[trans-4-(4'-chlorophenyl) cyclohexyl]-3-hydroxy-1,4-naphthoquinone (566C80). Biochem Pharmacol. **1992**;43(7):1545-53. Epub 1992/04/01. doi: 10.1016/0006-2952(92)90213-3. PubMed PMID: 1314606.

9. Painter HJ, Morrisey JM, Mather MW, Vaidya AB. Specific role of mitochondrial electron transport in blood-stage *Plasmodium falciparum*. Nature. **2007**;446(7131):88-91. doi: 10.1038/nature05572. PubMed PMID: 17330044.

10. Antonova-Koch Y, Meister S, Abraham M, Luth MR, Ottilie S, Lukens AK, Sakata-Kato T, Vanaerschot M, Owen E, Jado JC, Maher SP, Calla J, Plouffe D, Zhong Y, Chen K, Chaumeau V, Conway AJ, McNamara CW, Ibanez M, Gagaring K, Serrano FN, Eribez K, Taggard CM, Cheung AL, Lincoln C, Ambachew B, Rouillier M, Siegel D, Nosten F, Kyle DE, Gamo FJ, Zhou Y, Llinas M, Fidock DA, Wirth DF, Burrows J, Campo B, Winzeler EA. Open-source discovery of chemical leads for next-generation chemoprotective antimalarials. Science. **2018**;362(6419):eaat9446. Epub 2018/12/14. doi: 10.1126/science.aat9446. PubMed PMID: 30523084; PMCID: PMC6516198.

11. Paton DG, Childs LM, Itoe MA, Holmdahl IE, Buckee CO, Catteruccia F. Exposing Anopheles mosquitoes to antimalarials blocks *Plasmodium* parasite transmission. Nature. **2019**;567(7747):239-43. Epub 20190227. doi: 10.1038/s41586-019-0973-1. PubMed PMID: 30814727; PMCID: PMC6438179.

12. Nilsen A, LaCrue AN, White KL, Forquer IP, Cross RM, Marfurt J, Mather MW, Delves MJ, Shackleford DM, Saenz FE, Morrisey JM, Steuten J, Mutka T, Li Y, Wirjanata G, Ryan E, Duffy S, Kelly JX, Sebayang BF, Zeeman AM, Noviyanti R, Sinden RE, Kocken CHM, Price RN, Avery VM, Angulo-Barturen I, Jimenez-Diaz MB, Ferrer S, Herreros E, Sanz LM, Gamo FJ, Bathurst I, Burrows JN, Siegl P, Guy RK, Winter RW, Vaidya AB, Charman SA, Kyle DE, Manetsch R, Riscoe MK. Quinolone-3-diarylethers: a new class of antimalarial drug. Sci Transl Med. **2013**;5(177):177ra37. doi: 10.1126/scitranslmed.3005029. PubMed PMID: 23515079; PMCID: PMC4227885.

13. Simao-Gurge RM, Wunderlich G, Cricco JA, Cubillos EFG, Domenech-Carbo A, Cebrian-Torrejon G, Almeida FG, Cirulli BA, Katzin AM. Biosynthesis of heme O in intraerythrocytic stages of Plasmodium falciparum and potential inhibitors of this pathway. Sci Rep. **2019**;9(1):19261. Epub 20191217. doi: 10.1038/s41598-019-55506-y. PubMed PMID: 31848371; PMCID: PMC6917786.

14. Ke HJ, Morrisey JM, Ganesan SM, Painter HJ, Mather MW, Vaidya AB. Variation among *Plasmodium falciparum* Strains in Their Reliance on Mitochondrial Electron Transport Chain Function. Eukaryot Cell. **2011**;10(8):1053-61. doi: 10.1128/Ec.05049-11. PubMed PMID: WOS:000293383000006.

15. Falekun S, Sepulveda J, Jami-Alahmadi Y, Park H, Wohlschlegel JA, Sigala PA. Divergent acyl carrier protein decouples mitochondrial Fe-S cluster biogenesis from fatty acid synthesis in malaria parasites. Elife. **2021**;10:e71636. Epub 20211006. doi: 10.7554/eLife.71636. PubMed PMID: 34612205; PMCID: PMC8547962.

16. Espino-Sanchez TJ, Wienkers H, Marvin RG, Nalder SA, Garcia-Guerrero AE, VanNatta PE, Jami-Alahmadi Y, Mixon Blackwell A, Whitby FG, Wohlschlegel JA, Kieber-Emmons MT, Hill CP, Sigala PA. Direct tests of cytochrome c and c(1) functions in the electron transport chain of malaria parasites. Proc Natl Acad Sci U S A. **2023**;120(19):e2301047120. Epub 20230501. doi: 10.1073/pnas.2301047120. PubMed PMID: 37126705; PMCID: PMC10175771.

17. Skinner-Adams TS, Fisher GM, Riches AG, Hutt OE, Jarvis KE, Wilson T, von Itzstein M, Chopra P, Antonova-Koch Y, Meister S, Winzeler EA, Clarke M, Fidock DA, Burrows JN, Ryan JH, Andrews KT. Cyclization-blocked proguanil as a strategy to improve the antimalarial activity of atovaquone. Commun Biol. **2019**;2:166. Epub 20190503. doi: 10.1038/s42003-019-0397-3. PubMed PMID: 31069275; PMCID: PMC6499835.

18. Babbitt SE, Sutherland MC, San Francisco B, Mendez DL, Kranz RG. Mitochondrial cytochrome c biogenesis: no longer an enigma. Trends Biochem Sci. **2015**;40(8):446-55. Epub 20150611. doi: 10.1016/j.tibs.2015.05.006. PubMed PMID: 26073510; PMCID: PMC4509832.

19. Hamel P, Corvest V, Giege P, Bonnard G. Biochemical requirements for the maturation of mitochondrial c-type cytochromes. Biochim Biophys Acta. **2009**;1793(1):125-38. Epub 20080704. doi: 10.1016/j.bbamcr.2008.06.017. PubMed PMID: 18655808.

20. Stevens JM, Daltrop O, Allen JW, Ferguson SJ. C-type cytochrome formation: chemical and biological enigmas. Acc Chem Res. **2004**;37(12):999-1007. Epub 2004/12/22. doi: 10.1021/ar030266l. PubMed PMID: 15609992.

21. Flegontov P, Michalek J, Janouskovec J, Lai DH, Jirku M, Hajduskova E, Tomcala A, Otto TD, Keeling PJ, Pain A, Obornik M, Lukes J. Divergent mitochondrial respiratory chains in phototrophic relatives of apicomplexan parasites. Mol Biol Evol. **2015**;32(5):1115-31. Epub 20150206. doi: 10.1093/molbev/msv021. PubMed PMID: 25660376.

22. Dumont ME, Ernst JF, Hampsey DM, Sherman F. Identification and sequence of the gene encoding cytochrome c heme lyase in the yeast Saccharomyces cerevisiae. EMBO J. **1987**;6(1):235-41. doi: 10.1002/j.1460-2075.1987.tb04744.x. PubMed PMID: 3034577; PMCID: PMC553382.

23. San Francisco B, Bretsnyder EC, Kranz RG. Human mitochondrial holocytochrome c synthase's heme binding, maturation determinants, and complex formation with cytochrome c. Proc Natl Acad Sci U S A. **2013**;110(9):E788-97. Epub 20121112. doi: 10.1073/pnas.1213897109. PubMed PMID: 23150584; PMCID: PMC3587199.

24. Sutherland MC, Mendez DL, Babbitt SE, Tillman DE, Melnikov O, Tran NL, Prizant NT, Collier AL, Kranz RG. In vitro reconstitution reveals major differences between human and bacterial cytochrome c synthases. Elife. **2021**;10. Epub 20210511. doi: 10.7554/eLife.64891. PubMed PMID: 33973521; PMCID: PMC8112865.

25. Bernard DG, Gabilly ST, Dujardin G, Merchant S, Hamel PP. Overlapping specificities of the mitochondrial cytochrome c and c1 heme lyases. J Biol Chem. **2003**;278(50):49732-42. Epub 20030926. doi: 10.1074/jbc.M308881200. PubMed PMID: 14514677.

26. Zollner A, Rodel G, Haid A. Molecular cloning and characterization of the Saccharomyces cerevisiae CYT2 gene encoding cytochrome-c1-heme lyase. Eur J Biochem. **1992**;207(3):1093-100. doi: 10.1111/j.1432-1033.1992.tb17146.x. PubMed PMID: 1499554.

27. Tjhin ET, Hayward JA, McFadden GI, van Dooren GG. Characterization of the apicoplast-localized enzyme TgUroD in Toxoplasma gondii reveals a key role of the apicoplast in heme biosynthesis. J Biol Chem. **2020**;295(6):1539-50. Epub 20191230. doi: 10.1074/jbc.RA119.011605. PubMed PMID: 31914409; PMCID: PMC7008375.

28. Bushell E, Gomes AR, Sanderson T, Anar B, Girling G, Herd C, Metcalf T, Modrzynska K, Schwach F, Martin RE, Mather MW, McFadden GI, Parts L, Rutledge GG, Vaidya AB, Wengelnik K, Rayner JC, Billker O. Functional Profiling of a *Plasmodium* Genome Reveals an Abundance of Essential Genes. Cell. **2017**;170(2):260-72 e8. doi: 10.1016/j.cell.2017.06.030. PubMed PMID: 28708996; PMCID: PMC5509546.

29. Zhang M, Wang C, Otto TD, Oberstaller J, Liao X, Adapa SR, Udenze K, Bronner IF, Casandra D, Mayho M, Brown J, Li S, Swanson J, Rayner JC, Jiang RHY, Adams JH. Uncovering the essential genes of the human malaria parasite *Plasmodium falciparum* by saturation mutagenesis. Science. **2018**;360(6388):eaap7847. Epub 2018/05/05. doi: 10.1126/science.aap7847. PubMed PMID: 29724925; PMCID: PMC6360947.

30. Posayapisit N, Songsungthong W, Koonyosying P, Falade MO, Uthaipibull C, Yuthavong Y, Shaw PJ, Kamchonwongpaisan S. Cytochrome c and c1 heme lyases are essential in *Plasmodium berghei*. Mol Biochem Parasitol. **2016**;210(1-2):32-6. Epub 20160809. doi: 10.1016/j.molbiopara.2016.08.003. PubMed PMID: 27520480.

31. Babbitt SE, San Francisco B, Bretsnyder EC, Kranz RG. Conserved residues of the human mitochondrial holocytochrome c synthase mediate interactions with heme. Biochemistry. **2014**;53(32):5261-71. Epub 20140806. doi: 10.1021/bi500704p. PubMed PMID: 25054239; PMCID: PMC4139152.

32. Mendez DL, Babbitt SE, King JD, D'Alessandro J, Watson MB, Blankenship RE, Mirica LM, Kranz RG. Engineered holocytochrome c synthases that biosynthesize new cytochromes c. Proc Natl Acad Sci U S A. **2017**;114(9):2235-40. Epub 20170214. doi: 10.1073/pnas.1615929114. PubMed PMID: 28196881; PMCID: PMC5338485.

33. Abramson J, Adler J, Dunger J, Evans R, Green T, Pritzel A, Ronneberger O, Willmore L, Ballard AJ, Bambrick J, Bodenstein SW, Evans DA, Hung CC, O'Neill M, Reiman D, Tunyasuvunakool K, Wu Z, Zemgulyte A, Arvaniti E, Beattie C, Bertolli O, Bridgland A, Cherepanov A, Congreve M, Cowen-Rivers AI, Cowie A, Figurnov M, Fuchs FB, Gladman H, Jain R, Khan YA, Low CMR, Perlin K, Potapenko A, Savy P, Singh S, Stecula A, Thillaisundaram A, Tong C, Yakneen S, Zhong ED, Zielinski M, Zidek A, Bapst V, Kohli P, Jaderberg M, Hassabis D, Jumper JM. Accurate structure prediction of biomolecular interactions with AlphaFold 3. Nature. **2024**. Epub 20240508. doi: 10.1038/s41586-024-07487-w. PubMed PMID: 38718835.

34. Zhang Y, Stevens JM, Ferguson SJ. Substrate recognition of holocytochrome c synthase: N-terminal region and CXXCH motif of mitochondrial cytochrome c. FEBS Lett. **2014**;588(18):3367-74. Epub 20140730. doi: 10.1016/j.febslet.2014.07.026. PubMed PMID: 25084480; PMCID: PMC4158909.

35. Babbitt SE, San Francisco B, Mendez DL, Lukat-Rodgers GS, Rodgers KR, Bretsnyder EC, Kranz RG. Mechanisms of mitochondrial holocytochrome c synthase and the key roles played by cysteines and histidine of the heme attachment site, Cys-XX-Cys-His. J Biol Chem. **2014**;289(42):28795-807. Epub 20140828. doi: 10.1074/jbc.M114.593509. PubMed PMID: 25170082; PMCID: PMC4200240.

36. Lill R, Stuart RA, Drygas ME, Nargang FE, Neupert W. Import of cytochrome c heme lyase into mitochondria: a novel pathway into the intermembrane space. EMBO J. **1992**;11(2):449-56. doi: 10.1002/j.1460-2075.1992.tb05074.x. PubMed PMID: 1371459; PMCID: PMC556474.

37. Ganesan SM, Falla A, Goldfless SJ, Nasamu AS, Niles JC. Synthetic RNA-protein modules integrated with native translation mechanisms to control gene expression in malaria parasites. Nat Commun. **2016**;7:10727. Epub 20160301. doi: 10.1038/ncomms10727. PubMed PMID: 26925876; PMCID: PMC4773503.

38. Maruthi M, Ling L, Zhou J, Ke H. Dispensable Role of Mitochondrial Fission Protein 1 (Fis1) in the Erythrocytic Development of Plasmodium falciparum. mSphere. **2020**;5(5). Epub 20200923. doi: 10.1128/mSphere.00579-20. PubMed PMID: 32968006; PMCID: PMC7568643.

39. Okada M, Rajaram K, Swift RP, Mixon A, Maschek JA, Prigge ST, Sigala PA. Critical role for isoprenoids in apicoplast biogenesis by malaria parasites. Elife. **2022**;11:eLife.73208. Epub 20220308. doi: 10.7554/eLife.73208. PubMed PMID: 35257658; PMCID: PMC8959605.

40. Evers F, Cabrera-Orefice A, Elurbe DM, Kea-Te Lindert M, Boltryk SD, Voss TS, Huynen MA, Brandt U, Kooij TWA. Composition and stage dynamics of mitochondrial complexes in *Plasmodium falciparum*. Nat Commun. **2021**;12(1):3820. Epub 20210621. doi: 10.1038/s41467-021-23919-x. PubMed PMID: 34155201; PMCID: PMC8217502.

41. Maclean AE, Bridges HR, Silva MF, Ding S, Ovciarikova J, Hirst J, Sheiner L. Complexome profile of *Toxoplasma gondii* mitochondria identifies divergent subunits of respiratory chain complexes including new subunits of cytochrome bc1 complex. PLoS Pathog. **2021**;17(3):e1009301. Epub 20210302. doi: 10.1371/journal.ppat.1009301. PubMed PMID: 33651838; PMCID: PMC7987180.

42. Hayward JA, Rajendran E, Zwahlen SM, Faou P, van Dooren GG. Divergent features of the coenzyme Q:cytochrome c oxidoreductase complex in *Toxoplasma gondii* parasites. PLoS Pathog. **2021**;17(2):e1009211. Epub 20210201. doi: 10.1371/journal.ppat.1009211. PubMed PMID: 33524071; PMCID: PMC7877769.

43. Sheokand P, Muhleip A, Sheiner L. Plasmodium falciparum mitochondrial complex III, the target of atovaquone, is essential for progression to the transmissible sexual stages. bioRxiv. **2024**. Epub January 9, 2024. doi: https://doi.org/10.1101/2024.01.09.574740.

44. Balta VA, Stiffler D, Sayeed A, Tripathi AK, Elahi R, Mlambo G, Bakshi RP, Dziedzic AG, Jedlicka AE, Nenortas E, Romero-Rodriguez K, Canonizado MA, Mann A, Owen A, Sullivan DJ, Prigge ST, Sinnis P, Shapiro TA. Clinically relevant atovaquone-resistant human malaria parasites fail to transmit by mosquito. Nat Commun. **2023**;14(1):6415. Epub 20231012. doi: 10.1038/s41467-023-42030-x. PubMed PMID: 37828012; PMCID: PMC10570281.

45. Goodman CD, Siregar JE, Mollard V, Vega-Rodriguez J, Syafruddin D, Matsuoka H, Matsuzaki M, Toyama T, Sturm A, Cozijnsen A, Jacobs-Lorena M, Kita K, Marzuki S, McFadden GI. Parasites resistant to the antimalarial atovaquone fail to transmit by mosquitoes. Science. **2016**;352(6283):349-53. doi: 10.1126/science.aad9279. PubMed PMID: 27081071; PMCID: PMC5149070.

46. Zhang Z, Huang L, Shulmeister VM, Chi YI, Kim KK, Hung LW, Crofts AR, Berry EA, Kim SH. Electron transfer by domain movement in cytochrome bc1. Nature. **1998**;392(6677):677-84. Epub 1998/05/16. doi: 10.1038/33612. PubMed PMID: 9565029.

47. Crivellone MD, Wu MA, Tzagoloff A. Assembly of the mitochondrial membrane system. Analysis of structural mutants of the yeast coenzyme QH2-cytochrome c reductase complex. J Biol Chem. **1988**;263(28):14323-33. PubMed PMID: 2844766.

48. Nicholson DW, Stuart RA, Neupert W. Biogenesis of cytochrome c1. Role of cytochrome c1 heme lyase and of the two proteolytic processing steps during import into mitochondria. J Biol Chem. **1989**;264(17):10156-68. PubMed PMID: 2542325.

49. Muhleip A, Kock Flygaard R, Ovciarikova J, Lacombe A, Fernandes P, Sheiner L, Amunts A. ATP synthase hexamer assemblies shape cristae of Toxoplasma mitochondria. Nat Commun. **2021**;12(1):120. Epub 20210105. doi: 10.1038/s41467-020-20381-z. PubMed PMID: 33402698; PMCID: PMC7785744.

50. Hillier C, Pardo M, Yu L, Bushell E, Sanderson T, Metcalf T, Herd C, Anar B, Rayner JC, Billker O, Choudhary JS. Landscape of the Plasmodium Interactome Reveals Both Conserved and Species-Specific Functionality. Cell Rep. **2019**;28(6):1635-47 e5. doi: 10.1016/j.celrep.2019.07.019. PubMed PMID: 31390575; PMCID: PMC6693557.

51. Kranz RG, Richard-Fogal C, Taylor JS, Frawley ER. Cytochrome c biogenesis: mechanisms for covalent modifications and trafficking of heme and for heme-iron redox control. Microbiol Mol Biol Rev. **2009**;73(3):510-28, Table of Contents. Epub 2009/09/02. doi: 10.1128/MMBR.00001-09. PubMed PMID: 19721088; PMCID: PMC2738134.

52. Allen JW, Jackson AP, Rigden DJ, Willis AC, Ferguson SJ, Ginger ML. Order within a mosaic distribution of mitochondrial c-type cytochrome biogenesis systems? FEBS J. **2008**;275(10):2385-402. Epub 20080403. doi: 10.1111/j.1742-4658.2008.06380.x. PubMed PMID: 18393999.

53. Holm L, Rosenstrom P. Dali server: conservation mapping in 3D. Nucleic Acids Res. **2010**;38(Web Server issue):W545-9. Epub 20100510. doi: 10.1093/nar/gkq366. PubMed PMID: 20457744; PMCID: PMC2896194.

54. Ke H, Sigala PA, Miura K, Morrisey JM, Mather MW, Crowley JR, Henderson JP, Goldberg DE, Long CA, Vaidya AB. The heme biosynthesis pathway is essential for *Plasmodium falciparum* development in mosquito stage but not in blood stages. J Biol Chem. **2014**;289(50):34827-37. Epub 20141028. doi: 10.1074/jbc.M114.615831. PubMed PMID: 25352601; PMCID: PMC4263882.

55. Nagaraj VA, Sundaram B, Varadarajan NM, Subramani PA, Kalappa DM, Ghosh SK, Padmanaban G. Malaria parasite-synthesized heme is essential in the mosquito and liver stages and complements host heme in the blood stages of infection. PLoS Pathog. **2013**;9(8):e1003522. Epub 20130801. doi: 10.1371/journal.ppat.1003522. PubMed PMID: 23935500; PMCID: PMC3731253.

56. Rizopoulos Z, Matuschewski K, Haussig JM. Distinct Prominent Roles for Enzymes of Plasmodium berghei Heme Biosynthesis in Sporozoite and Liver Stage Maturation. Infect Immun. **2016**;84(11):3252-62. Epub 20161017. doi: 10.1128/IAI.00148-16. PubMed PMID: 27600503; PMCID: PMC5067757.

57. Goldberg DE, Sigala PA. *Plasmodium* heme biosynthesis: To be or not to be essential? PLoS Pathog. **2017**;13(9):e1006511. Epub 20170928. doi: 10.1371/journal.ppat.1006511. PubMed PMID: 28957449; PMCID: PMC5619821.

58. Rathnapala UL, Goodman CD, McFadden GI. A novel genetic technique in Plasmodium berghei allows liver stage analysis of genes required for mosquito stage development and demonstrates that de novo heme synthesis is essential for liver stage development in the malaria parasite. PLoS Pathog. **2017**;13(6):e1006396. Epub 20170615. doi: 10.1371/journal.ppat.1006396. PubMed PMID: 28617870; PMCID: PMC5472305.

59. Sigala PA, Crowley JR, Henderson JP, Goldberg DE. Deconvoluting heme biosynthesis to target blood-stage malaria parasites. Elife. **2015**;4:e09143. Epub 20150714. doi: 10.7554/eLife.09143. PubMed PMID: 26173178; PMCID: PMC4532139.

60. Medlock AE, Shiferaw MT, Marcero JR, Vashisht AA, Wohlschlegel JA, Phillips JD, Dailey HA. Identification of the Mitochondrial Heme Metabolism Complex. PLoS One. **2015**;10(8):e0135896. Epub 20150819. doi: 10.1371/journal.pone.0135896. PubMed PMID: 26287972; PMCID: PMC4545792.

61. Piel RB, 3rd, Dailey HA, Jr., Medlock AE. The mitochondrial heme metabolon: Insights into the complex(ity) of heme synthesis and distribution. Mol Genet Metab. **2019**;128(3):198-203. Epub 20190117. doi: 10.1016/j.ymgme.2019.01.006. PubMed PMID: 30709775; PMCID: PMC6640082.

62. Spillman NJ, Beck JR, Ganesan SM, Niles JC, Goldberg DE. The chaperonin TRiC forms an oligomeric complex in the malaria parasite cytosol. Cell Microbiol. **2017**;19(6):cmi.12719. Epub 20170124. doi: 10.1111/cmi.12719. PubMed PMID: 28067475; PMCID: PMC5429184.

63. Wellems TE, Panton LJ, Gluzman IY, do Rosario VE, Gwadz RW, Walker-Jonah A, Krogstad DJ. Chloroquine resistance not linked to mdr-like genes in a *Plasmodium falciparum* cross. Nature. **1990**;345(6272):253-5. Epub 1990/05/17. doi: 10.1038/345253a0. PubMed PMID: 1970614.

64. Ponnudurai T, Leeuwenberg AD, Meuwissen JH. Chloroquine sensitivity of isolates of *Plasmodium falciparum* adapted to in vitro culture. Trop Geogr Med. **1981**;33(1):50-4. Epub 1981/03/01. PubMed PMID: 7018038.

65. van den Hoff MJ, Moorman AF, Lamers WH. Electroporation in 'intracellular' buffer increases cell survival. Nucleic Acids Res. **1992**;20(11):2902. doi: 10.1093/nar/20.11.2902. PubMed PMID: 1614888; PMCID: PMC336954.

66. Lowry OH, Rosebrough NJ, Farr AL, Randall RJ. Protein measurement with the Folin phenol reagent. J Biol Chem. **1951**;193(1):265-75. PubMed PMID: 14907713.

67. Altschul SF, Madden TL, Schaffer AA, Zhang J, Zhang Z, Miller W, Lipman DJ. Gapped BLAST and PSI-BLAST: a new generation of protein database search programs. Nucleic Acids Res. **1997**;25(17):3389-402. doi: 10.1093/nar/25.17.3389. PubMed PMID: 9254694; PMCID: PMC146917.

68. Sievers F, Higgins DG. Clustal Omega, accurate alignment of very large numbers of sequences. Methods Mol Biol. **2014**;1079:105-16. doi: 10.1007/978-1-62703-646-7_6. PubMed PMID: 24170397.

69. Waterhouse AM, Procter JB, Martin DM, Clamp M, Barton GJ. Jalview Version 2--a multiple sequence alignment editor and analysis workbench. Bioinformatics. **2009**;25(9):1189-91. Epub 20090116. doi: 10.1093/bioinformatics/btp033. PubMed PMID: 19151095; PMCID: PMC2672624.

70. Jumper J, Evans R, Pritzel A, Green T, Figurnov M, Ronneberger O, Tunyasuvunakool K, Bates R, Zidek A, Potapenko A, Bridgland A, Meyer C, Kohl SAA, Ballard AJ, Cowie A, Romera-Paredes B, Nikolov S, Jain R, Adler J, Back T, Petersen S, Reiman D, Clancy E, Zielinski M, Steinegger M, Pacholska M, Berghammer T, Bodenstein S, Silver D, Vinyals O, Senior AW, Kavukcuoglu K, Kohli P, Hassabis D. Highly accurate protein structure prediction with AlphaFold. Nature. **2021**;596(7873):583-9. Epub 20210715. doi: 10.1038/s41586-021-03819-2. PubMed PMID: 34265844; PMCID: PMC8371605.

71. DeLano WL. MacPyMOL: A PyMOL-based Molecular Graphics Application for MacOS X. Palo Alto, CA: DeLano Scientific LLC; 2007.

SUPPORTING INFORMATION
(Figures S1-S11 and Table S1)

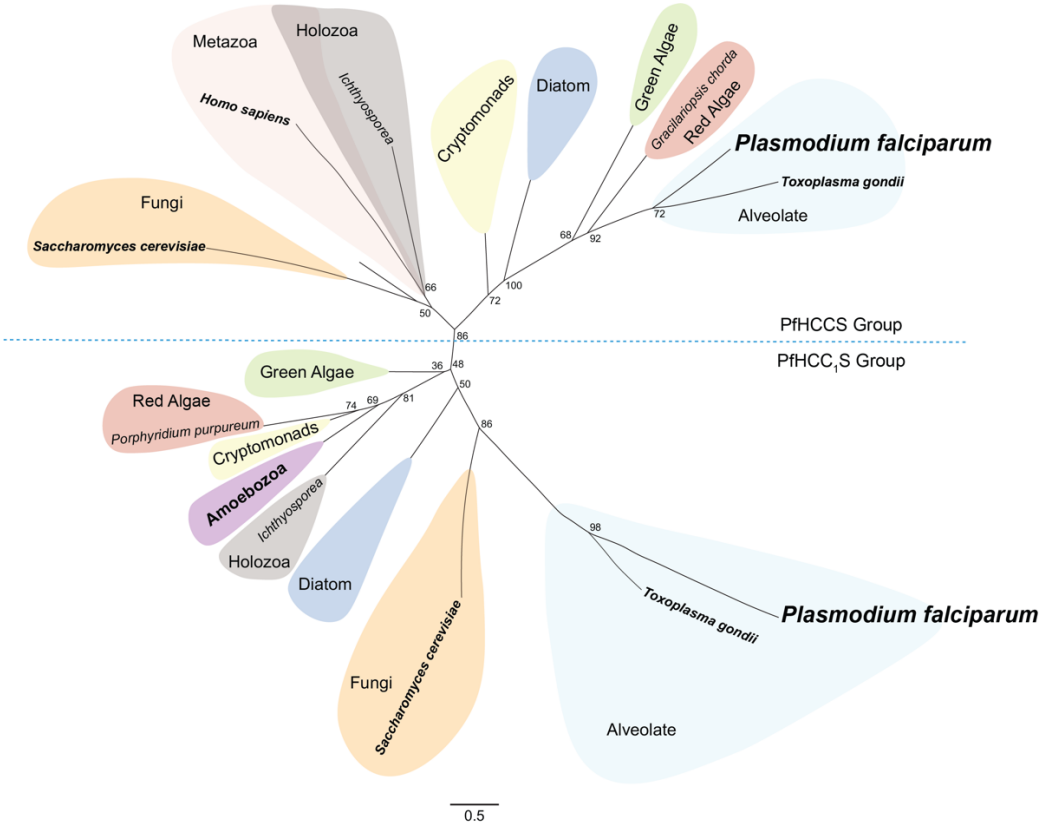

Figure S1. Molecular phylogeny of *P. falciparum* HCCS and HCC_1S. BLAST analysis was used to identify orthologs of *P. falciparum* HCCS and HCC_1S, with alignment of 52 sequences for construction of a Maximum Likelihood phylogenetic tree. Bootstrap values are indicated at branch points. The scale bar corresponds to the expected sequence changes per 100 residues. The raw phylogenetic tree is shown in **Fig. S12**.

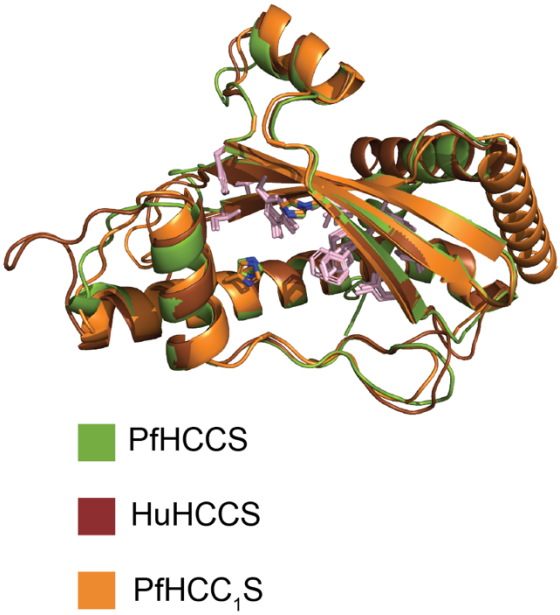

Figure S2. Structural alignment of the AlphaFold models *P. falciparum* HCCS, *P. falciparum* HCC_1S, and human HCCS.

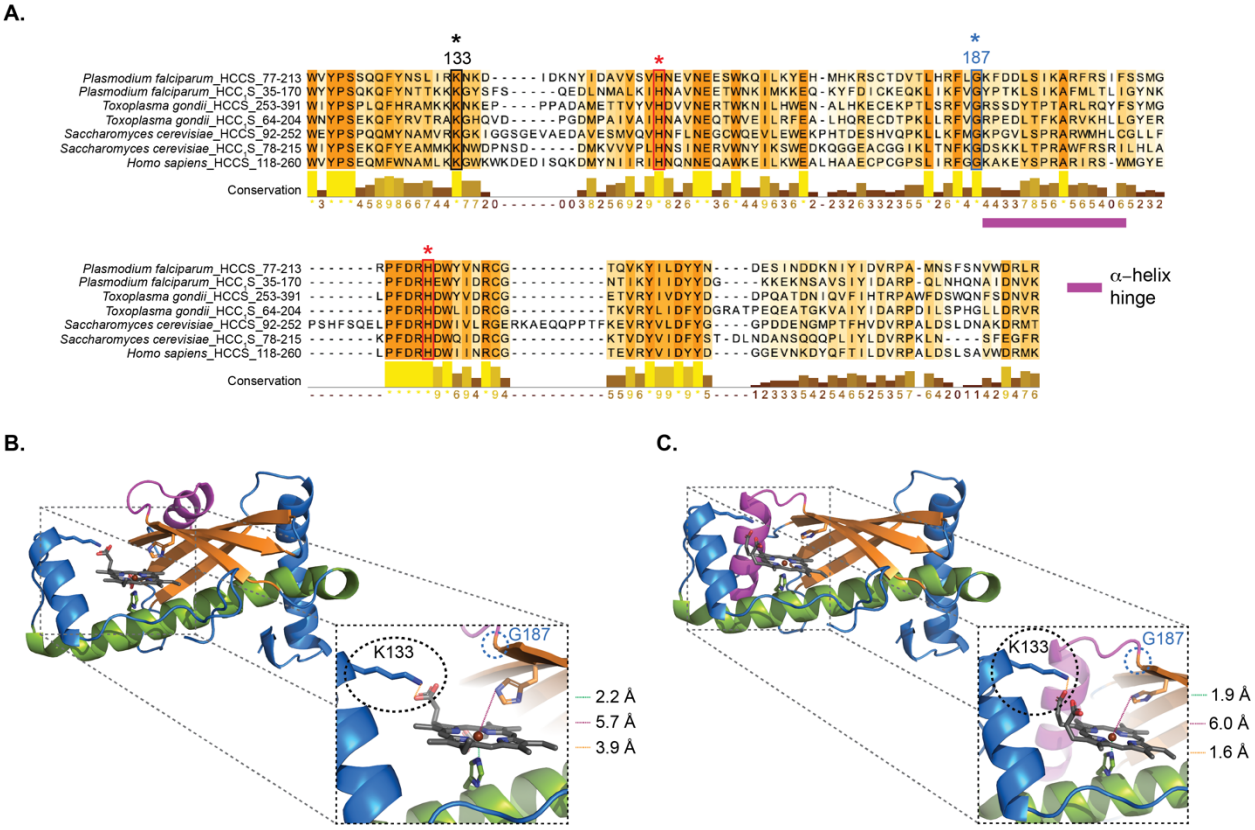

Figure S3. Sequence conservation and conformational dynamics of HCCS. (A) Sequence alignment of parasite, yeast, and human HCCS homologs highlighting conservation of K92 and G140 (human numbering). (B) and (C) AlphaFold-predicted structural models for *P. falciparum* HCCS with central alpha helix in two distinct conformations that expose (B) or occlude (C) the heme-binding pocket.

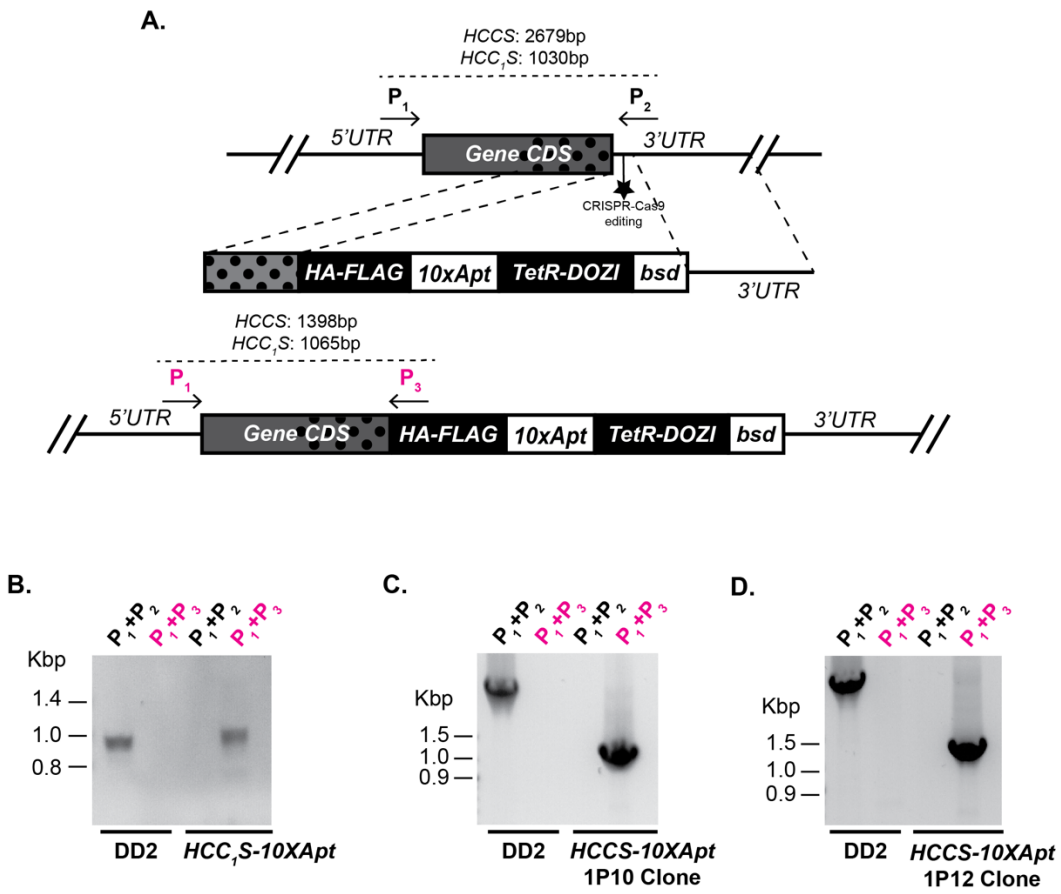

Figure S4. Genotyping HCC_1S and HCCS integrations in Dd2 parasites. (A) Schematic model for editing the chromosomal gene for *P. falciparum* HCCS and HCC_1S to encode a C-terminal HA-FLAG epitope tag fusion and the aptamer/TetR-DOZI system. PCR primer sites are indicated with a "P" along with expected amplicon sizes for primer pairs. (B) Genotype PCR for parental and polyclonal transfectants to edit HCC_1S. (C-D) Genotype PCR for parental and clonal transfectants to edit HCCS.

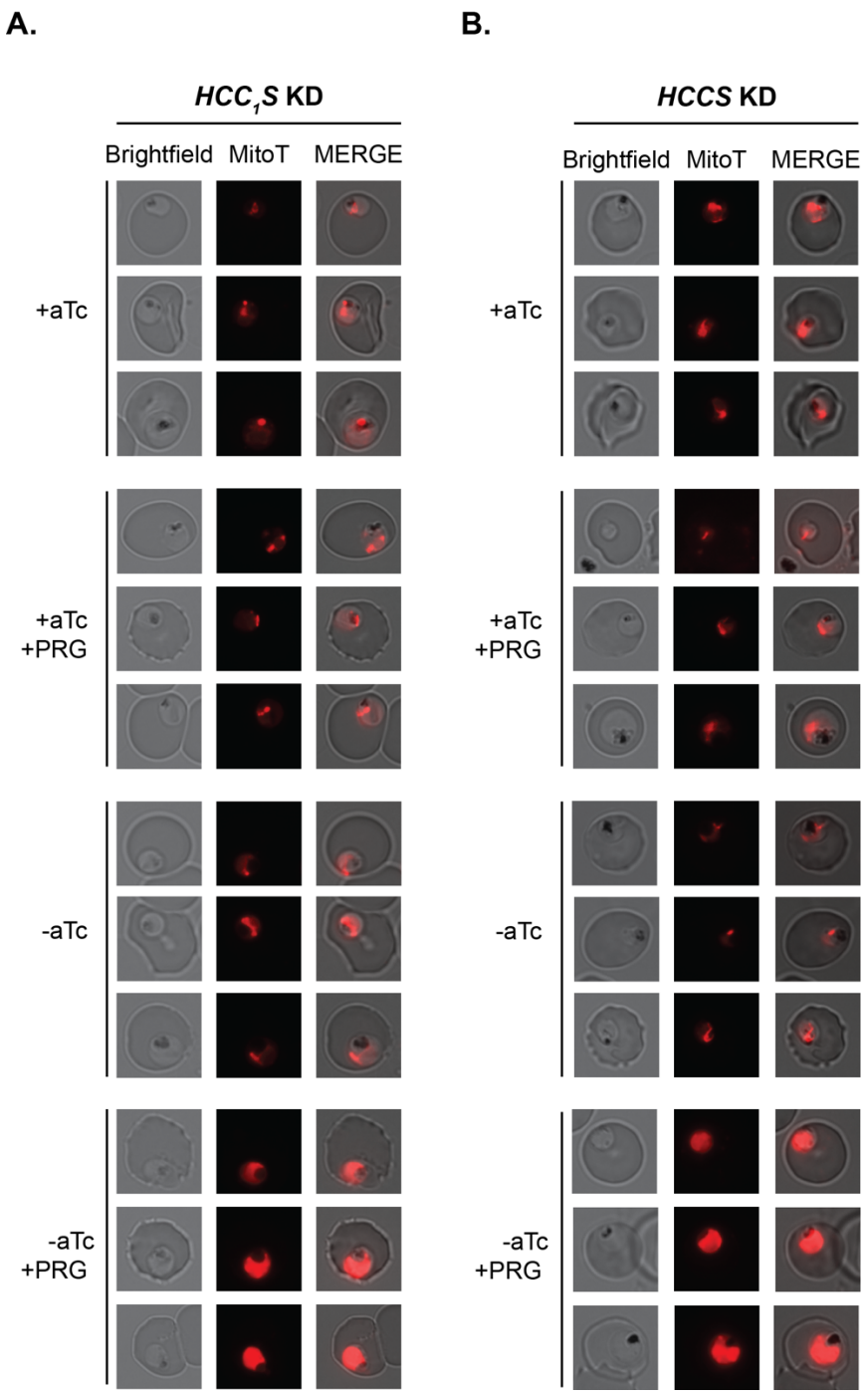

Figure S5. Additional live-parasite microscopy images of HCC_1S (A) and HCCS (B) aptamer/TetR-DOZI Dd2 parasites cultured 5 days ±aTc/+dQ and 1 μM proguanil (PRG) and stained with 1 nM with MitoTracker Red (MitoT).

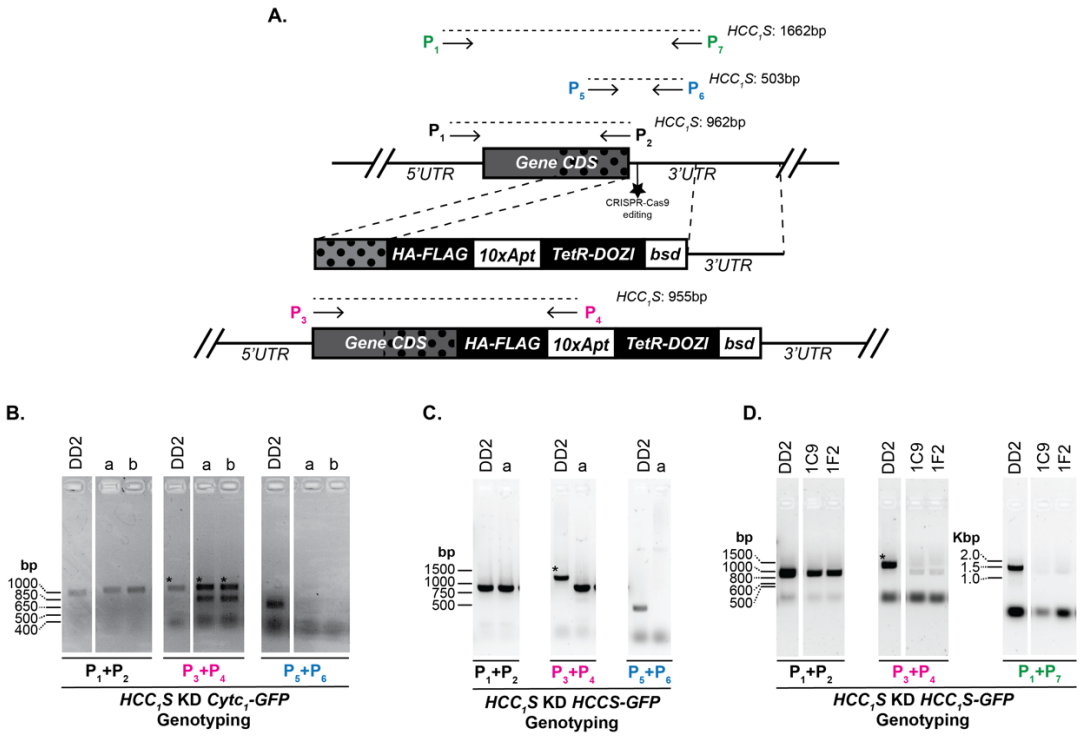

Figure S6. Genotyping HCC_1S integrations in Dd2 parasites transfected with plasmids for episomal expression. (A) Schematic model for editing the chromosomal gene for *P. falciparum* HCC_1S to encode a C-terminal HA-FLAG epitope tag fusion and the 10x aptamer/TetR-DOZI system. PCR primer sites are indicated with a "P" along with expected amplicon sizes for primer pairs. (B) Genotype PCR for parental and polyclonal transfectants (a and b) to edit HCC_1S in parasites transfected with a plasmid for episomal expression of cyt c_1-GFP. (C) Genotype PCR for parental and polyclonal transfectant a to edit HCC_1S in parasites transfected with a plasmid for episomal expression of HCCS-GFP. (D) Genotype PCR for parental and clonal transfectants 1C9 and 1F2 to edit HCC_1S in parasites transfected with a plasmid for episomal expression of HCC_1S-GFP. Non-specific amplicons are indicated with asterisks.

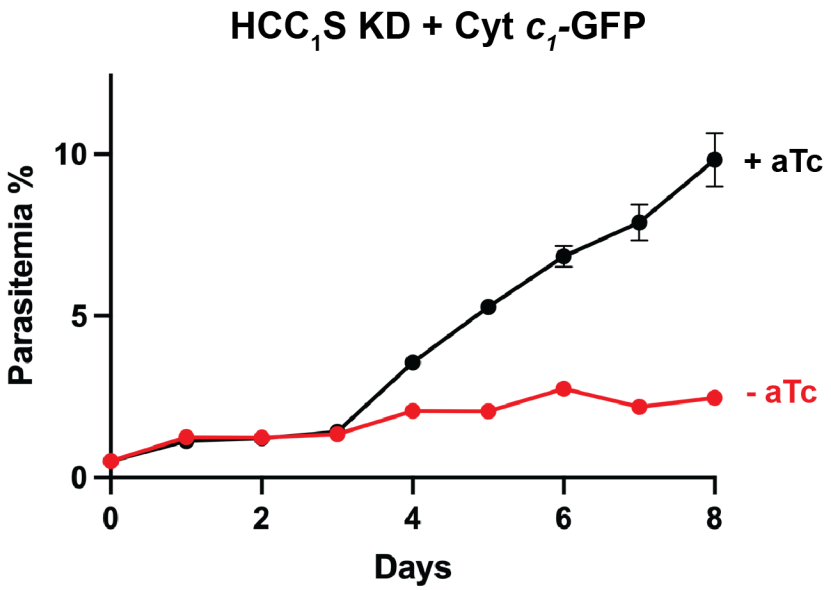

Figure S7. Synchronous growth assay of Dd2 parasites tagged for conditional knockdown (KD) of HCC_1S expression in ±anhydrotetracycline (aTc) conditions and transfected with a plasmid for episomal expression of cyt c_1-GFP. Data points and error bars represent the average ± SD of biological triplicates.

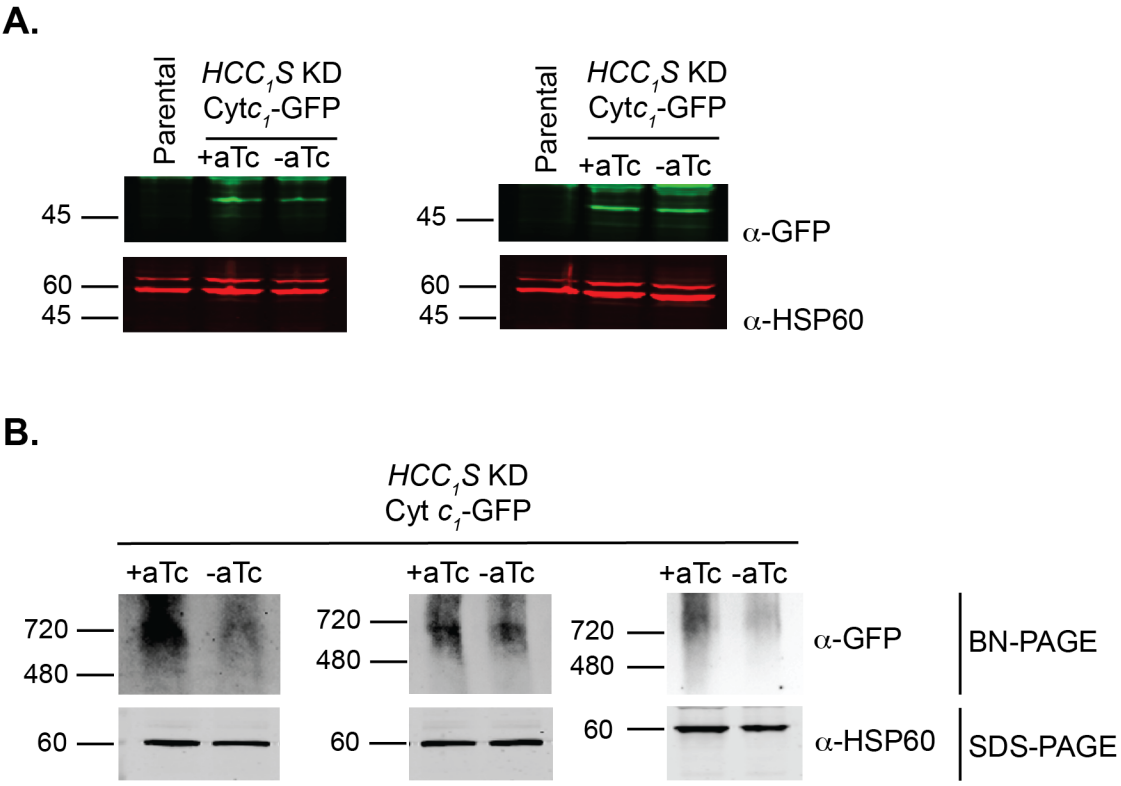

Figure S8. Additional western blot (WB) images from biological replicate growth assays of HCC_1S knockdown Dd2 parasites episomally expressing cyt c_1-GFP and grown 3 days ±aTc . (A) SDS-PAGE/WB images from independent growth assays (left and right) probed with α-GFP (green) and α-Hsp60 (red) antibodies. (B) Blue native-PAGE/WB analysis of cyt c_1-GFP and SDS-PAGE/WB analysis of HSP60 expression levels in HCC_1S knockdown parasites cultured 5 days ±aTc/+dQ. 20 µg of total protein from mitochondrial lysates were loaded for each lane. Blots were probed with α-GFP or α-HSP60 antibodies.

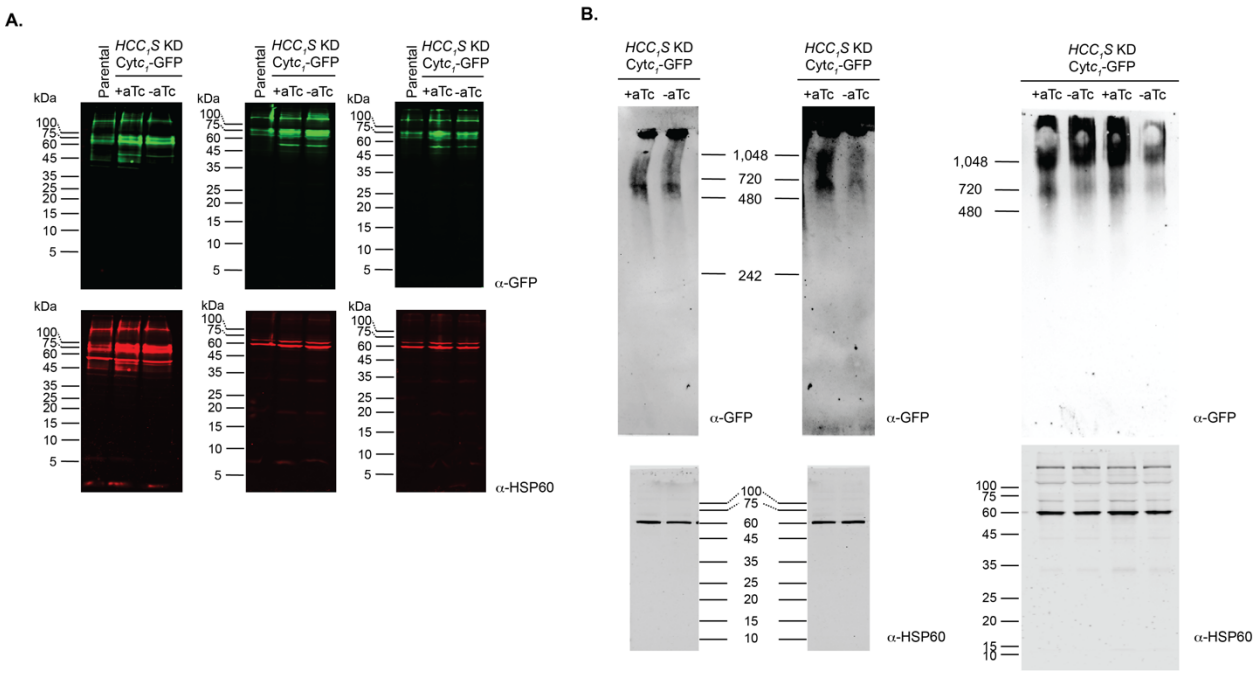

Figure S9. Uncropped images of (A) SDS-PAGE/WB and (B) BN-PAGE/WB analyses of cyt c_1-GFP levels in HCC_1S knockdown (KD) Dd2 parasites cultured in ±aTc/+dQ conditions.

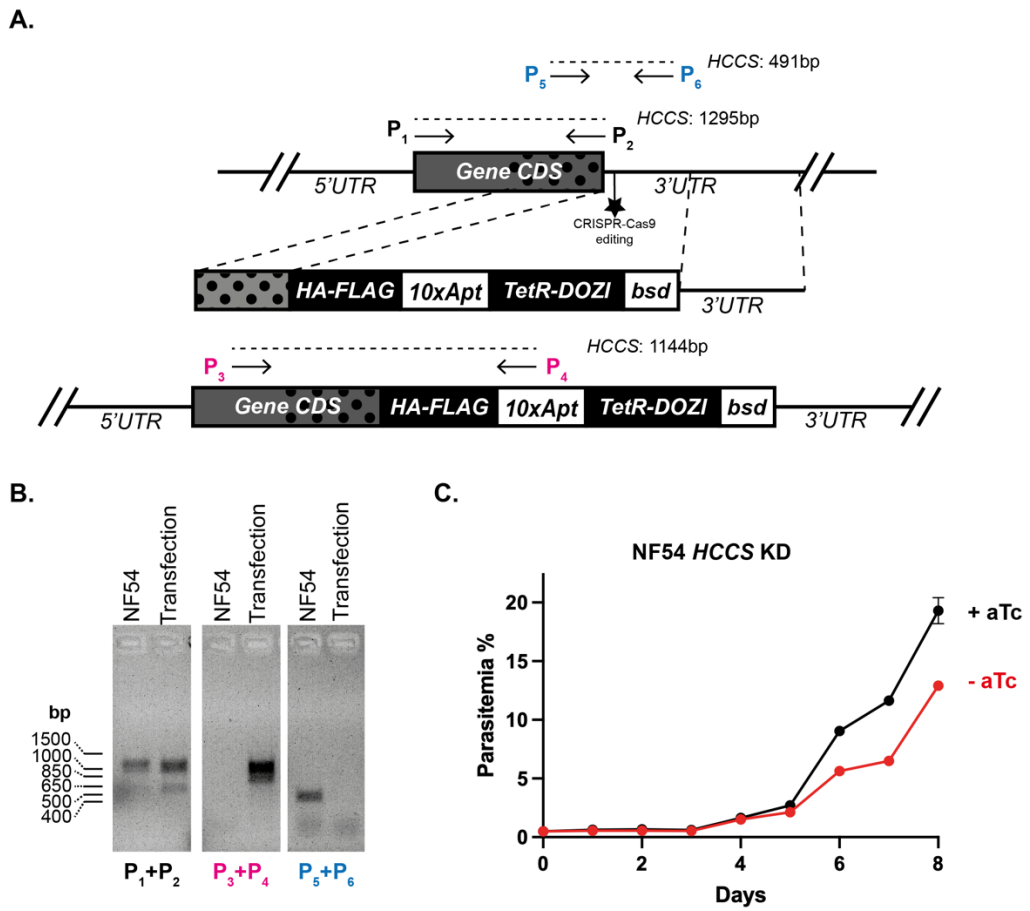

Figure S10. Genotyping HCCS integration in NF54 parasites. (A) Schematic model for editing the chromosomal gene for *P. falciparum* HCCS to encode a C-terminal HA-FLAG epitope tag fusion and the aptamer/TetR-DOZI system. PCR primer sites are indicated with a "P" along with expected amplicon sizes for primer pairs. (B) Genotype PCR for parental and polyclonal transfectants to edit HCC_1S. (C) Synchronous growth assay of NF54 parasites tagged for conditional knockdown (KD) of HCCS expression in ±anhydrotetracycline (aTc) conditions. Data points and error bars represent the average ± SD of biological triplicates.

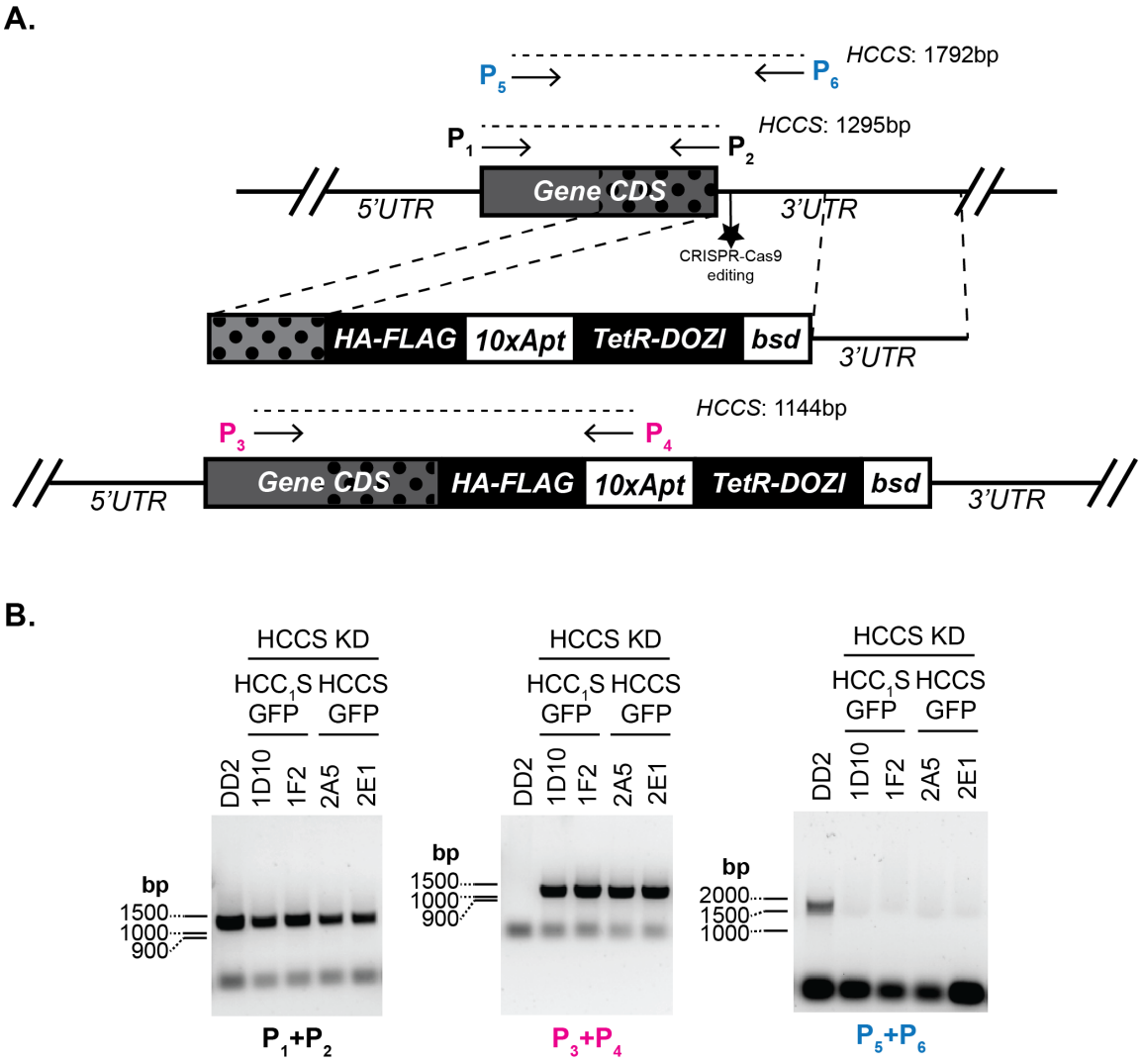

Figure S11. Genotyping HCCS integrations in Dd2 parasites transfected with plasmids for episomal expression. (A) Schematic model for editing the chromosomal gene for *P. falciparum* HCCS to encode a C-terminal HA-FLAG epitope tag fusion and the 10x aptamer/TetR-DOZI system. PCR primer sites are indicated with a "P" along with expected amplicon sizes for primer pairs. (B) Genotype PCR for parental and clonal transfectants to edit HCCS in parasites episomal expressing HCC_1S-GFP or HCCS-GFP.

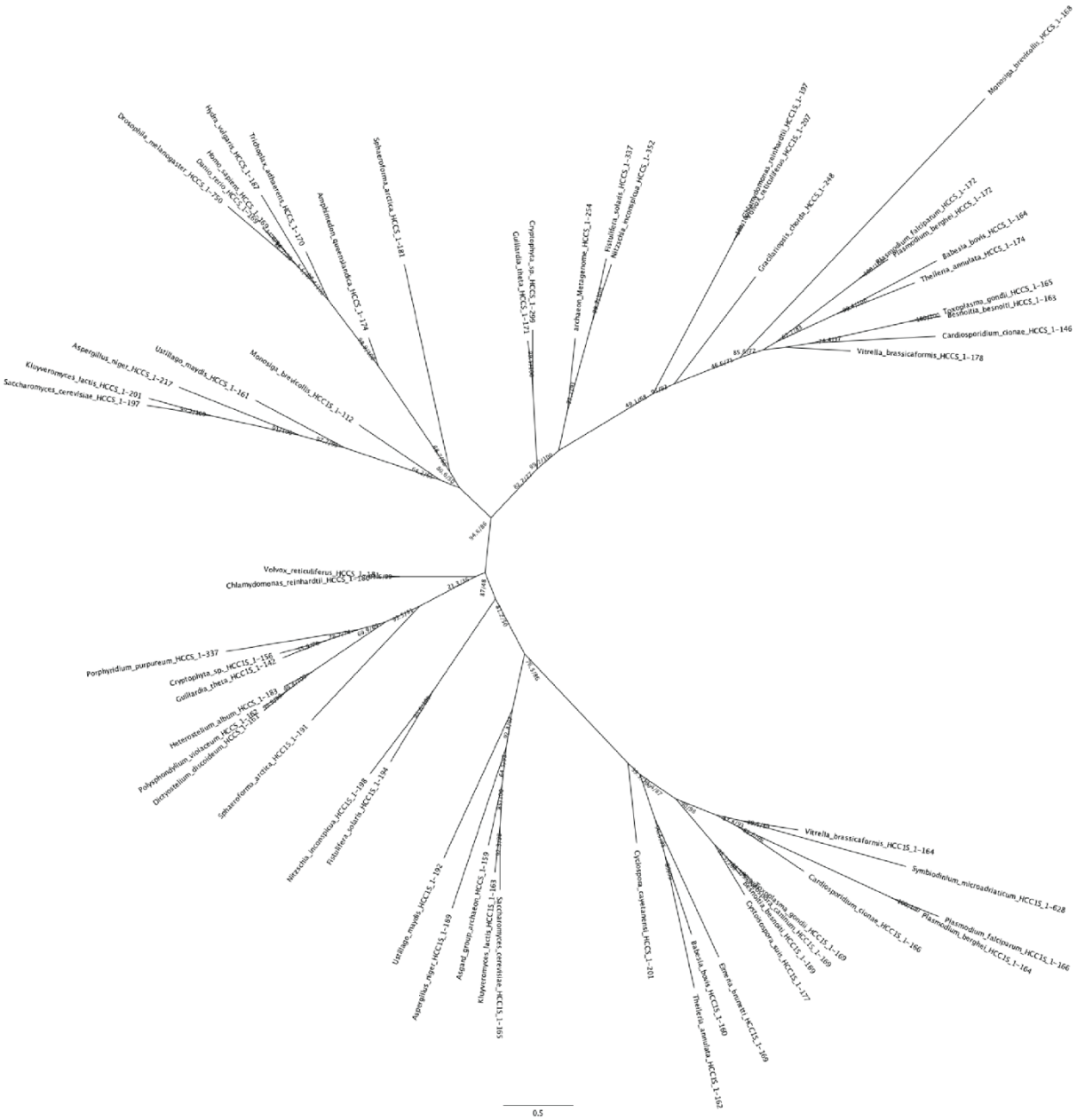

Figure S12. Raw phylogenetic tree based on sequence comparison of *P. falciparum* HCCS and HCC_1S relative to diverse eukaryotes.

Table S1. List of primers.

Primer	Sequence	
#51	CCCCTTTCCGGGCGCGCCGTATGTATTGAATACATTTGTTTCG	AscI restriction site
#52	CGGGCATCATATTTCTTTCGCTTAAGCCTTTATTTATTTGTATATGTGCATAAATAAATG	AflII restriction site
#53	CATTTATTTATGCACATATACAAATAAATAAAGGCTTAAGCGAAAGAAATATGATGCCCG	AflII restriction site
#54	CATAAGGATAGACGTCTTTAAATAATTCATCTTTTTTTACATACTTAAAG	AatII restriction site
#55	CCCCTTTCCGGGCGCGCCCTTTCTTTTTGTGCATCATAAATG	AscI restriction site
#56	TATATTTTCTTTTTTTTGTTCATTCATCTTAAGGTAATTCTGTATTAACAAAAACATATC	AflII restriction site
#57	GATATGTTTTTGTTAATACAGAATTACCTTAAGATGAATGAACAAAAAAAGAAAATATA	AflII restriction site
#58	CATAAGGATAGACGTCAAAAAGGTTATTTAAAAATCTACAAATCTTTATATAAATAATTTTAAC	AatII restriction site
Primers for gRNAs		
HCCS_gRNA1_F	TAAGTATATAATATTTAACAAAAATTGTGAAAAATGTTTTAGAGCTAGAA	gRNA sequence in red
HCCS_gRNA1_R	TTCTAGCTCTAAAACATTTTTCACAATTTTTGTTAGCAATATTATATACTTA	
HCCS_gRNA2_F	TAAGTATATAATATTGCAAATGTGCAACAAACAATGTTTTAGAGCTAGAA	gRNA sequence in red
HCCS_gRNA2_R	TTCTAGCTCTAAAACATTGTTTGTTGCACATTTGCGCAATATTATATACTTA	
HCC1S_gRNA_F	TAAGTATATAATATTTTATTTATATAAAGATTTGTGTTTTAGAGCTAGAA	gRNA sequence in red
HCC1S_gRNA_R	TTCTAGCTCTAAAACACAAATCTTTATATAAATAAGCAATATTATATACTTA	
Primers for genotyping		
#77_P1	CTTATAAGGAACAAAAGCGAAATAAATAAATATGCAGAATTTAAGTCCAGC	To genotype *HCCS* KD
#52_P2	CGGGCATCATATTTCTTTCGCTTAAGCCTTTATTTATTTGTATATGTGCATAAATAAATG	To genotype *HCCS* KD
#83_P3	CCCAGGCCTCTAGTTTAC	To genotype *HCCS* KD
#86_P1	CAACTTAAAAGAAAAAAAATTAAATCATATAAAGAAAAAATATAC	To genotype *HCC$_1$S* KD
#58_P2	CATAAGGATAGACGTCAAAAAGGTTATTTAAAAATCTACAAATCTTTATATAAATAATTTTAAC	To genotype *HCC$_1$S* KD
#57_P3	GATATGTTTTTGTTAATACAGAATTACCTTAAGATGAATGAACAAAAAAAGAAAATATA	To genotype *HCC$_1$S* KD
#83_P4	CCCAGGCCTCTAGTTTAC	To genotype *HCC$_1$S* KD
PfHCC$_1$S Fw1_P5	TTCTGCAGTCTCAATTTATATTGATGCCAGACCA	To genotype *HCC$_1$S* KD
PfHCC$_1$S Rv1_P6	ATGTAAATTTAACAAATCTGTTAAAAATATATGAACGAAATAA	To genotype *HCC$_1$S* KD
PfHCC$_1$S Rv4_P7	GACAAGAATATACTTGGCGCAAATTAATTATATATACATACC	To genotype *HCC$_1$S* KD
Primers for RT-qPCR		
HCCS_qF1	TGGGATGTTCAGATGGAACGAA	
HCCS_qR1	AGACATTGGGAATCTCGGGC	
HCC$_1$S_qF1	AGTTGGTACTATCCATCCCAGA	
HCC$_1$S_qR1	AATCTTCTTGAGAGAAGGAGTAACC	
GFP_qF1	TCTGTCAGTGGAGAGGGTGA	
GFP_qR1	AGTGTTGGCCATGGAACAGG	
I5P_qF1	GACATAAGTTTAGTAGGTCG	
I5P_qR1	TTCTGACTCCACATCATTTG	
ADSL_qF1	GGAAATCCATAGACAAACAATG	
ADSL_qR1	TCCTGTGAGAAGTGCTCCAC	